**KASDI MERBAH UNIVERSITY – OUARGLA**
**FACULTY OF HYDROCARBONS, RENEWABLE ENERGY**
**And EARTH AND UNIVERSE SCIENCES**
**DEPARTMENT OF EARTH SCIENCES AND THE UNIVERSONO**

**Academic Master's Thesis**
**Field: Earth and Universe Sciences**
**Branch: Geology Speciality: Sedimentary Basins**

## THEME

# LITHOSPHERIC AND ASTHENOSPHERIC PROPERTIES OF THE SAHARAN PLATFORM INFERRED FROM POTENTIAL FIELD, GEOID

**Presented by :**

**Publicly supported on**

**Before the jury: President:**

**Promoter:**

**Co-Promoter**

**Examiner:**

**University year 2023/2024**

# Gifting andappreciation

The locomotive of the research went through many obstacles, yet I tried to overcome them steadily by the grace of God. To my parents, siblings, and friends, they have been a great support to me in completing the research. I should not forget my professors who played the biggest role in supporting me and providing me with valuable information. .... I dedicate my graduation research to you ..... May Allah Almighty prolong your lives and bless you with good things.

# SUMMARY

# Lists of figures

# LISTS OF FIGURES

# Lists of tables

# INTRODUCTION

## 1-Introduction :

The estimation of geothermal potential is primarily influenced by certain geodynamic conditions and processes that shape the crust, upper and lower mantle Geothermal fields with reservoir temperatures greater than 90°C have been associated with Albian hydrothermal systems that occur at ~900 to 1700 m within the Algerian Saharan platform (Saibi, 2009; Melouah 2021). Previous thermo-geophysical models have defined the continental lithosphere within the cratonic basins of the Sahara to be devoid of significant tectonic and magmatic events in recent past. The Saharan platform that is flanked by the West African craton and Saharan metacraton, is host to several Triassic basins. These basins are affected by N-S/NE-SW bound faults, filled with ~2000 to 7000 m Mesozoic-Cenozoic sediments. Studies have shown that the Triassic basin has significant geothermal resource potential (Melouah 2021; Elbarbary 2022) Previous studies demonstrated that the area is characterized by regional geothermal fields (Kedaid 2007; Saibi, 2009), hot water reservoirs, and structural fabrics of thermal reservoirs (Melouah 2021; Elbarbary 2022). Several researchers have reported the relationship that exists between deep structures of the upper mantle and thermal potentials of the region (Eldosouky et 2022; Chai 2022). Factors such as the Moho depth, lithosphere-asthenosphere thermal disequilibrium and radioactive heat production emanating from the upper mantle, have been observsed to influence the distribution of Curie depth isotherm. These factors provide the key for interpreting the origin of geothermal anomalies and understanding its genetic mechanism in sedimentary basins (Melouah 2021; La Rosa .2021; Alrefaee 2022).

In the Algerian Sahara, there is significant uncertainty with regards to the crust-mantle structure. Hence, the need for this comprehensive research is to close the geothermal resource knowledge gap and classify its genesis in relation to geodynamic activities within the Saharan platform. Major geothermal potentials are located in the southeastern Sahara (the Triassic province). The proximity of the potential zones of heat production from economic activity zones and urban areas is an important consideration when developing geothermal resources for energy generation, as this can reduce considerably, costs and efforts of energy transfer.

This study seeks to integrate anomalies from gravity, geoid, elevation, topography and heat flow information to generate realistic models of density, temperature and seismic wave velocity (P and S) distributions across the crust/uppermost mantle layers. This thermal-geophysical model can improve the thermo-tectonic knowledge of the crust/mantle structures

# CHAPITRE I :
# PRESENTATION OF THE STUDY AREA

# CHAPITRE I PRESENTATION OF THE STUDY AREA

## I . 1. Geological Framework of the Region:

Approaching the Sahara from the North, one transitions from the mountains and plateaux of the Atlas to the Saharan desert platform. This transition is marked by outcrops of sub-vertical white limestone, which correspond to what is known as the South Atlas Fault Zone. Depending on location, this fault zone may manifest as a fold, a fault-fold combination, or a flexure. South of this fault line—stretching from Agadir to the Gulf of Gabès—lies the African Shield composed predominantly of igneous and metamorphic rocks overlain by several thousand meters of sedimentary strata ranging from Cambrian to Quaternary periods (Cornet, 1964). This area can be subdivided into two sub-domains: the western basin and eastern basin, divided by the M'Zab anticline.

Our study area falls within this vast eastern sedimentary basin—a region that has occupied what is now Northern Sahara since at least Secondary times (Gouscov, 1952)

## I .2 Regional geology :

The Algerian geologic province can be categorized into northern structural domains comprising the folded Alpine region and the southern Saharan platform, with the Atlas flexure zone between these domains. Several geothermal and hydrocarbon reservoirs have been identified within sedimentary basins flanking the Saharan platform, which has been reported to be tectonically stable over time.

The Triassic basin, often considered an intracratonic basin and the most prolific within the eastern Algerian province, is situated within the Great Eastern Erg of the Sahara. Its evolution can be traced to regional deformation activities characterized by the Saharan platform. Four dominant phases of evolution have been identified, including collisional tectonics of the WAC and East African domain, Hercynian tectonic episodes, Trias-Lias rifting, and Austrian compression. The basin is overlain by thick deposits of Miocene-Pliocene and Mesozoic ages and is characterized by the Triassic-Liassic evaporite as a regional seal. Trapping mechanisms include stratigraphic, structural, and a combination of both, with relics of the Triassic associated with Archean dendritic assemblages overlain by evaporites, showing evidence of angular unconformity with Cambrian-Early Devonian formations

### I .3 Geological Structure of the Eastern Basin

The Eastern Basin (Fig1) of the Sahara, with sedimentary cover ranging from the Paleozoic to the Recent, is better understood than its western counterpart, thanks to petroleum exploration. It is bounded to the west by the M'zab Ridge and to the south by the Tadmaït and Tinrhert plateaus, dipping eastward into Tunisia and Libya. At its base lie folded Paleozoic sediments, shaped by the Hercynian orogeny, overlain unconformably by diverse Secondary and Tertiary sediments (marine and continental) to a thickness of approximately 2000 meters. The Eastern Basin also appears as a vast syncline, open to the north. In its southern half, this syncline is crossed by a major north-south-trending anticlinal ridge, hosting several oil fields, notably the Amguid-El Biod high. This ridge is no longer apparent in the Mio-Pliocene formations; there is even relief inversion, as the axis of the current Mio-Pliocene syncline superimposes on the old high. In the northern Sahara Basin, a second high zone existed from the Cenomanian to the Mio-Pliocene, between Hassi-Messaoud and the Tunisian border. This structure is oriented east-west, separating the chotts trough to the north from the rest of the basin. It appears that this ridge plays an important role in the hydrogeology of the region.

The regional geology of West Africa (Fig. 1) comprises two dominant tectonic domains: the West African Craton (WAC), consisting of three metamorphic and magmatic Archean-Paleoproterozoic shields sandwiched between two cratonic-origin basins, and the Pan-African orogenic belt, mainly composed of series of tectono-thermal events. The Man-Leon Shield, constituting the southern component of the WAC, is dominated by the presence of Paleoproterozoic Birimian continental crust associated with smaller inliers, namely the Kenieba and Kayes. To the north, the Reguibat Shield and its farthest counterpart, the Anti-Atlas mountain range, delimit the region. These two shields (i.e., Man-Leo and Reguibat) are considered stable since 1700 Ma and are primarily composed of Archean cores towards the west-central Kedougou-Kenieba and the extreme north of the Anti-Atlas in the WAC, entirely consisting of Birimian crust, without any known occurrence of Archean crust. In addition to the interiors and shields, thick sedimentary successions cover the WAC basement (e.g., the Taoudeni and Tindouf basins), ranging mostly from late Mesoproterozoic to Paleozoic. However, recent studies have identified Paleoproterozoic sequences in the northern WAC. The eastern end of the WAC shares its boundary with the mobile Pan-African belt, which constitutes the Touareg and Benin-Nigeria shields and is overlain by Paleozoic sedimentary basins. The evolutionary trends of these belts can be attributed to tectonic collisional episodes that occurred within 600 Ma. Potential field studies have shown significant correlation with N-S trending Hoggar structures and provide evidence of lateral extensions beneath the Saharan platform and its adjacent basins. In general, the Algerian geological domain can be classified into northern structural domains, which include the folded Alpine region and the southern Saharan platform, with the Atlas flexural zone between these structural domains. Several geothermal and hydrocarbon reservoirs have been identified in sedimentary basins bordering the Saharan platform, whose tectonic stability has been reported over time.

The Triassic Basin, often considered an intracratonic basin and the most prolific basin of the eastern Algerian domain, is located in the eastern Grand Erg of the Sahara. The evolution of the Triassic basin can be attributed to regional deformation activities that characterized the Saharan platform. Four dominant phases of Triassic basin evolution have been identified: the collisional tectonics of the WAC and East African domain, the Hercynian tectonic episode identified by regional tectonic inversion and erosion events, the Triassic-Lias rift phase with dominant tilted blocks, syn-sedimentary faults, and sediment thinning, and finally, the Albian-Aptian contractional phase that influenced the Algerian Sahara, characterized by localized uplift and erosion of Cambrian structures. The Triassic province is overlain by approximately 400 and over 4000 meters of Miocene-Pliocene and Mesozoic deposits, respectively. The Triassic-Liasevaporite constitutes the regional seal in Triassic reservoirs, while interbedded clays provide seals for Paleozoic reservoirs. Triassic relics associated with Archean dendritic assemblage are overlain by evaporites and show signs of angular unconformity with Cambrian-Devonian formations. The Hercynian unconformity and Hettangian dolomites (Early Jurassic) respectively link the Triassic basin to the basement and top. Trapping mechanisms are stratigraphic, structural, and a combination of both.

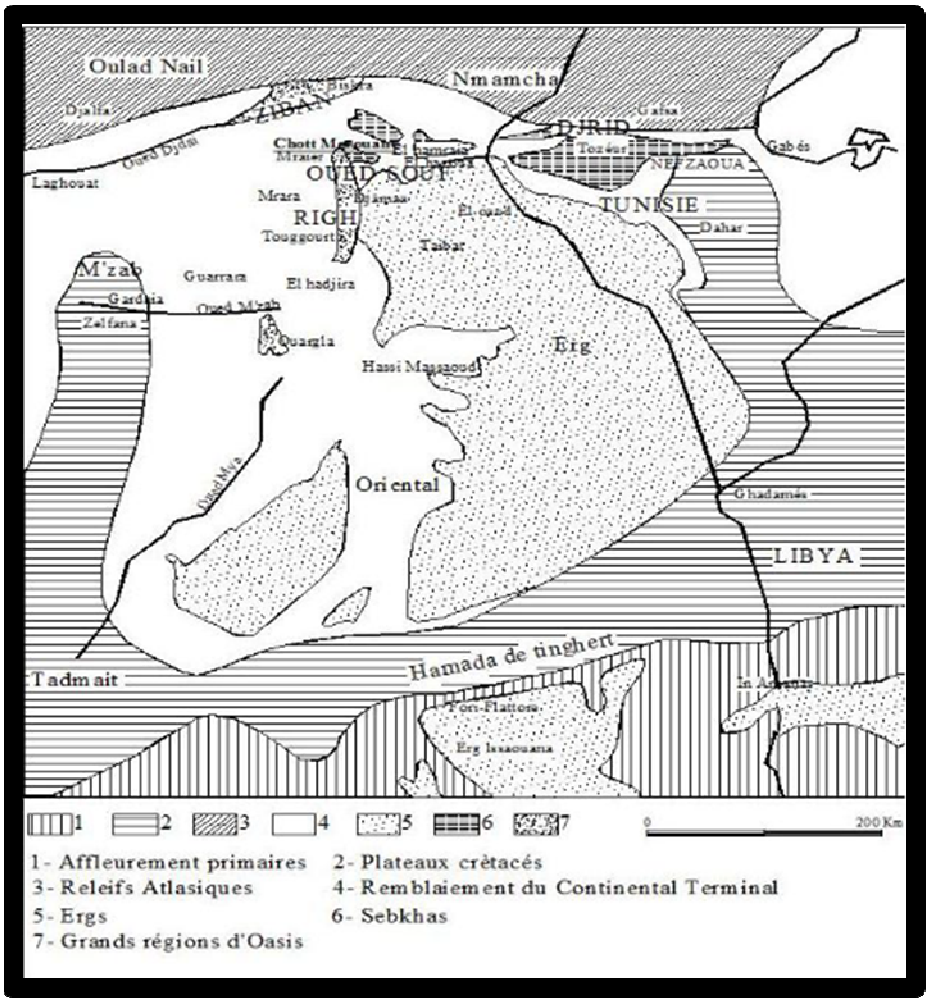


{**Figue1}:**The major geological units in the Sahara (Nesson, 1978)

## I 4. Lithostratigraphy:

**a**. Albian:

This stage includes a mass of sands and clays between the Aptian barrier and the overlying clay horizon attributed to the Cenomanian. It is noted that the change in sedimentary regime and the massive arrival of detrital sediments occurred between the Neocomian and the Barremian and during the Albian.

**b**. Vraconian:

The Vraconian is the transition term between the sandy Albian (top of the Continental Intercalaire) and the clay-carbonate Cenomanian (base of the Terminal Complex). It is represented by an irregular alternation of pelitic and dolomitic clay levels, sandy clays. It is

difficult to recognize in drilling, and the Vraconian has often been interpreted as either Albian or Cenomanian.

**c**. Cenomanian:

The Cenomanian consists of an alternation of dolomites, dolomitic limestones, clays, and anhydrite. The transition from the Vraconian to the Cenomanian is clear: a distinct sandy facies, attributed to the Albian, is followed by clays and evaporites attributed to the Cenomanian. In other drillings, the transition is less distinct: there is a transitional level attributed to the Vraconian. It seems reasonable, in this case, to choose the appearance of Cenomanian evaporites and dolomites as the upper limit of the Vraconian. The upper limit of the Cenomanian corresponds to the appearance of massive limestone or dolomite beds of the Turonian; it is always clear.

**d**. Turonian:

The Turonian consists of a thick bar of limestone and dolomite, which sharply contrasts with the evaporites and clays of the Cenomanian below and the Senonian above. Among all those in the eastern basin of the Algerian Sahara, the Turonian is the most well-characterized sedimentary formation. With a thickness ranging from about 25 to 70 meters in the study region, the Turonian consists of a thick bar of limestone and dolomite, sharply contrasting with the evaporites and clays of the Cenomanian below and the Senonian above.

Senonian:

It is differentiated into two facies: the lower Senonian (saline and anhydrite Senonian) with lagoon sedimentation characterized by clayey and saline formations with anhydrite, it is very impermeable. The upper Senonian (carbonate Senonian) is represented by permeable carbonate formations.

Tertiary:

**a** Eocene:

Two lithological sets are distinguished; the lower Eocene carbonate at the base, and the upper evaporitic Eocene.

- Lower carbonate Eocene: The carbonate Eocene is lithologically characterized, making it difficult to distinguish from the Senonian. The presence of nummulites is the only distinguishing criterion. Limestones tend to predominate over dolomites and evaporites. The latter are much rarer than in the Senonian, if not totally absent. Siliceous limestones encountered at the top of the carbonate Senonian continue into the Eocene. The thickness of this formation varies between 100 and 500 meters.

- Upper evaporitic Eocene: It consists of an alternation of limestone, anhydrite, and marls. Its thickness reaches about a hundred meters under the Chotts.

In the OuedRigh, the limestone aquifer seems to be located in a carbonate level belonging to the evaporitic Eocene.

**b** Miocene-Pliocene:

Bel and Demargne (1966) distinguish from bottom to top four levels in these lenticular deposits:

- Level 01: clayey, thin, existing only in the central zone of the Eastern Sahara along a North-South strip. These clays constitute a very impermeable barrier between the Senonian and the carbonate Eocene aquifer and that of the sands of level 02. Moving to level 03. It reaches 400 m south of GassiTouil. Level 02 is the main Miocene aquifer horizon.

- Level 03: It is a clayey-sandy formation whose lower and upper boundaries are quite poorly defined. This impermeable layer exists only in certain areas; it is thick and constant only in the region of the chotts.

- Level 04: This is the second sandy level of the Miocene. Sometimes continuous with level 02. The top of level 04 outcrops over large areas and is often made up of a crust of gritty limestone (Hamadian crust). The thickness of this horizon is about 300 m.

- Level 02: Sandy-gritty, this is the thickest and most consistent level; at its base, gravel is sometimes found, while the top gradually becomes clayey.

Quaternary:

It is essentially sandy, with clay and semi-permeable evaporite layers at the base.

This Quaternary formation is the origin of the formation of the groundwater table, mainly supplied by the infiltration of wadi waters and especially by percolation of excess waters during irrigation periods.

**e.** Eocene:

Two different lithological sets are distinguished, at the base: The carbonate Eocene is essentially formed by dolomites and dolomitic limestones with some intercalations of marls, clay, and even anhydrite and salt. The thickness of this formation varies between 100 and 500 m, with the maximum thickness in the lower Sahara zone. At the top, the evaporitic Eocene is formed by an alternation of limestone, anhydrite, and marls. Its thickness reaches about a hundred meters under the Chotts.

**f.** Mio-Plio-Quaternary:

The continental Tertiary of the Sahara can be relatively thick (150 m). It presents itself in the form of a sandy and clayey facies with gypsum. In the lower Sahara, lacustrine sedimentation occurs in the form of sandy and clayey series known as the Continental Terminal (Miocene-Pliocene), whose thickness can reach a few hundred meters in the region of the Algero-Tunisian Chotts. In the OuedRigh region, two aquifer levels are identified within the sands, separated by a clay layer in the middle (first and second OuedRigh aquifer). The whole is surmounted by the clayey-sandy and gypsum Plio-Quaternary resulting from sedimentation

in a lacustrine environment during the drying phase of lagoons and chotts.

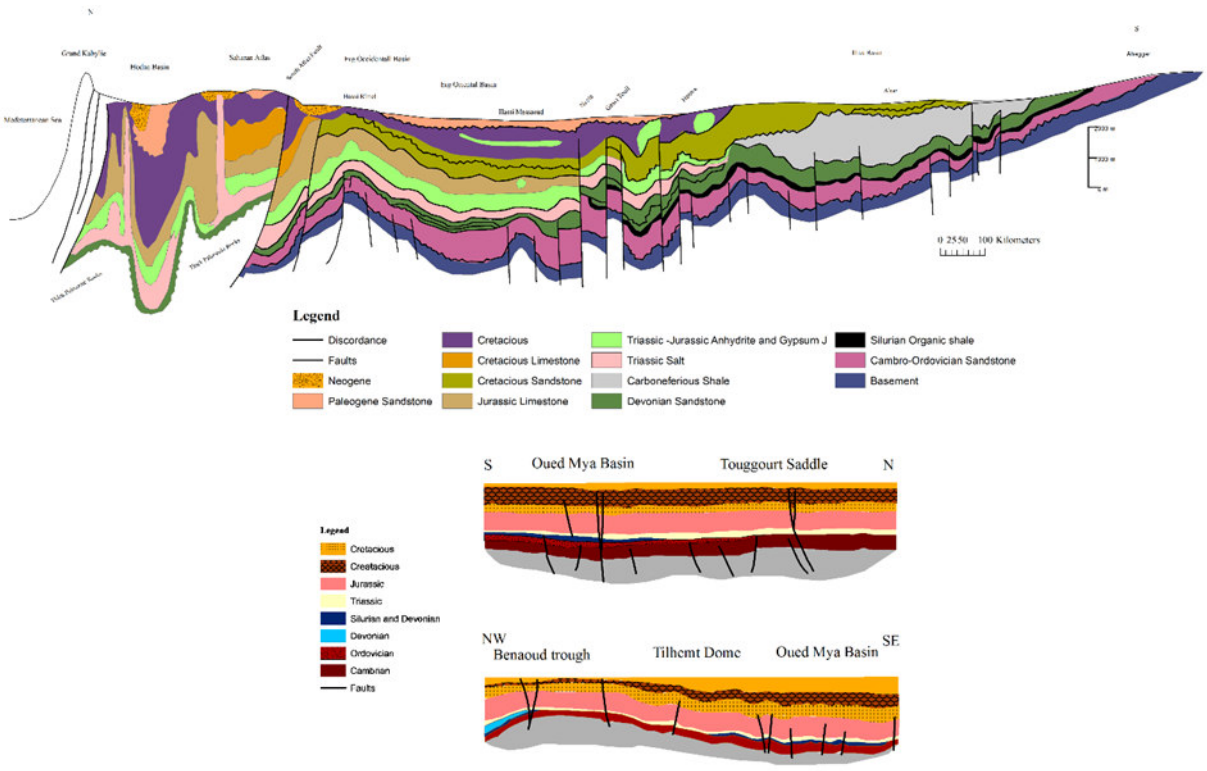


**[Fig.]:**Stratigraphic cross-section oriented in the N-S and NW-SE directions

## I.5. Regional Tectonics:

During the Secondary period, the eastern Algerian Sahara experienced overall vertical movements. While true mountain chains were forming further north in the Saharan Atlas geosyncline, the Saharan zone tended more towards a progressive collapse of its central part, following a dismissal roughly passing through the valley of OuedR'hir and the upper section of the Oued Mya valley.

The current geometry of the Continental Intercalaire and the Terminal Complex of the Sahara is characterized by the absence of significant tectonic deformations.

The Maghrebides chain, which underwent several orogenic phases during the Tertiary period, will have repercussions on the Saharan platform:

- The movements from the middle to upper Eocene are clear, followed by the lower Miocene phase which gives rise to the Tell and the Aurès.

- Finally, the Plio-Quaternary phase, which fits in with the previous ones in the Alpine phase; hence the appearance of fractures in the east-west direction, forming the uplift of the Aurès massif and the subsidence of the southern part, known as the "southern Aurès trough". These fractures govern the flow of groundwater, leading to the formation of chotts such as ChottMerouane and ChottMelghir. The east-west Atlasian flexure separates two distinct domains, resulting in the highest points in the north, the "Aurès Mountains", and the most depressed areas.

## I.6. Tectonics

### I.6. 1. The major stages of structural evolution from the Saharan platform to the Paleozoic.

Given the decrease in thickness sometimes even the complete disappearance of sedimentary units through local discordances or lack of sedimentation, it is necessary to recall the main phases of the structural evolution of the platformSaharan form during the Paleozoic.

I.6.1.1. Pan-African Orogenesis and the Origin of the North African Craton Fracturing Network.

Materialized by vertical movements accompanied by volcanic eruptions and uprisings, resulting in erosion of the sedimentary cover. The result of this orogenesis is the fracturing network.

I.6.1.2. Cambro-Ordovician distension and cover placement.

Resulting in the formation of a pediplane, called Infra-tassilian.

I.6.1.3. Taconic compression phase (Caradoc).

After the period of distension followed by the generalized transgression of Arenigian - Lianvirien, the Caradoc is witnessing a compressive movement, accompanied by regional uprisings leading to erosion. At the same time, there has been a climate change that has led to the establishment of an ice cap, centered in the central Sahara of Caradoc-Asligillien age.

I.6.1.4. Melting of the ice sheet and eustatic replays.

The melting of the ice sheet (the Upper Ordovician caused a rise in the sea level).

I.6.1.5. The Caledonian compression phase.

It took place at the end of the Silurian with an east-west orientation.

I.6.1.6. The distension phase of the Lower Devonian.

After the distensive movements, we witness a marine transgression the emsien.

I.6.1.7. Tectonic movements of the upper Middle Devonian.

Materialized by the Frasnian discordance, of north-south orientation.

I.6.1.8. Post-FaménnienMovement.

I.6.1.9. Hercynian Movements.

According to the study (A. BOUDJEMAA 1987), two Hercynian movements are highlighted:

I.6.1.9.1. Early Hercynian Movements.

At Tournaisien -viséen having a direction N40° of tightening.

I.6.1.9.2. Major Hercynian Movements.

Caused the Carboniferous sedimentation to stop completely. The axis of the folds and the measurements of the ridges give a clamping N120°.

The current architecture denotes a result of a long evolution, as the culmination of slow deformations that have continued more or less continuously throughout the history of the basin.

The main deformation phases influencing the sedimentation and structuring of the basin (Boeuf, 1971; Boudjemaa, 1987) are the Hercynian phase and the Austrian phase.

Hercynian movements correspond to a compression of direction

No. 120, the most significant deformation is along the NE-SW accidents.

One of the most important features of this formation concerns the fate of the main mother rocks (Silurian). They are preserved in the Berkine and OuedM'ya depressions, and will feed hydrocarbons into the structural and stratigraphic traps that will form later (Boudjemaa, 1987).

During the Austrian movements (aptien terminal), we witness an east-west compressive phase, which makes replay in reverse the subméridien accidents N-S of the OuedM'ya.

This compression would be responsible for the individualization of structural traps

### I.6.2. Structural Evolution of the Oued Mya Basin

The main structural elements are N-S and NE-SO. (SH and Sch ,2007).

In the Cambrian: There is a significant erosion that levels the structures and previous reliefs (Boeuf et al, 1971).

The OuedM'ya center perimeter was on the flank of a major depression that corresponded to the current location of the upper zone of HassiMessaoud (Benamrane, 1993).

The Ordovician begins with a marine transgression of the ArenigianLianvirinian, we witness regional uprisings (Eglab). These uprisings lead to erosion sometimes reaching the base (Boeuf, 1971). Towards the end of this period, a glaciation took place, with ice cap at the level of the current Hoggar.

Following the Caledonian phase, the area of OuedM'ya center began to rise while remaining submerged.

In the Silurian, the final melting of this ice cap leads to the rise of sea level, a widespread transgression reaches the southern Sahara where black graptolite clays are deposited (Boudjemaa, 1987).

At that time, the area of OuedM'yacentre was completely covered by this sea (Benamrane et al, 1993).

In the Devonian, following the tectonic uprising (Caledonian phase), a regression of the sea during the Géddinien, is followed by a transgression.

The beginning of the Hercynian orogenesis, and the gradual uprising of the HassiMessaoud area involved the displacement of the deposits from the center of the basin to the west, where the Devonian deposits are developed.

Towards the end of the Carboniferous, the collision between Gondwana and Laurasia accentuated the uplift of the Tilghermt dome area and the structuring of Djemaa-Touggourt.

The OuedM'ya region presented itself as a high submerged plateau, which prevented the deposition of the Carboniferous (Benamrane, et al, 1991) The Pangaea formation occurred near the end of the Hercynian orogenesis and the intense erosion of the reliefs reached the base in places.

At OuedM'ya the Devonian is the youngest Paleozoic formation. In the Permo-trias, the region remained continental until the end of the triassic, so that the Permian Sea did not reach the region.

The area of the OuedM'ya is characterized in the Triassic by a river system installed in favor of the paleo Hercynian valleys, according to the NE-SW direction with sources of contributions constituted by the high areas of the time, which are HassiR'mel, HassiMessaoud, and the vault of Allal.

At the end of the Triassic, the evaporitic deposits were followed by carbonates on this submerged land, then a marine transgression in the Upper Jurassic.

In the Cretaceous, a manifestation of alpine orogenesis, as well as a marine transgression settled on a large area followed by a regression to the Albian.

Following the widespread transgressions of the Cenomanian and Turonian, the Alpine orogenic movements have shaped the current structure.

The OuedM'ya area is currently characterized by a rather complex structure inherited from the Paleozoic, materialized by structural trends of NE-SW orientations.

# CHAPITRE II :

# modeling

# CHAPITRE II MODELING

## II . 1.Introduction

Estimation of geothermal potential is mainly influenced by certain conditionsand geodynamic processes that shape the crust, upper and lower mantle (Ai andal., 2021). Geothermal fields with reservoir temperatures above 90°Chave been associated with albian hydrothermal systems occurring at ~900 to 1700 min the Algerian Saharan platform (Saibi, 2009; Melouah et al., 2021a). Modelsprevious thermo-geophysics have defined the continental lithosphere in basinsSaharacratonics to be devoid of tectonic and magmatic eventssignificant in the recent past. The Saharan platform, flanked by the WestAfrican and Saharan metacraton, is home to several triassic basins. These basins areaffected by N-S/NE-SW linked faults, filled with mesozoic-cenozoic sediments of~2000 to 7000 m. Studies have shown that the triassic basin has potentialsignificant geothermal resources (Melouah et al., 2021a; Elbarbary et al., 2022).previous studies have shown that exists between deep mantle structureshigher and thermal potentials in the region (Eldosouky et 2022Chai 2022). Factors such as Moho depth, lithosphere thermal imbalance-asthenosphere and the production of radioactive heat emanating from the upper mantle wereobserved to influence the distribution of the Curie depth isotherm. These factorsprovide the key to interpreting the origin of geothermal anomalies and understanding itsgenetic mechanism in the sedimentary basins La Rosa In the Algerian Sahara, there is significant uncertainty regarding the structurecrust-mantle. Therefore, the need for this in-depth research is to fill thelack of knowledge about geothermal resources and classifying its genesis in relation togeodynamic activities within the Saharan platform. Significant potentialgeothermal are located in the southeast of the Sahara (that is, the province of Triassic). Theproximity of potential heat production areas from business areaseconomic and urban areas is an important consideration when developinggeothermal resources for energy production, as this can reduceenergy transfer costs and efforts. This study aims to integrateanomalies from information on gravity, geoid, altitude, topography andheat flow to generate realistic models of density, temperature andthe velocity of seismic waves (i.e. P and S) in the crust and mantle layerssuperior. This thermo-geophysical model can improve thermo-tectonic knowledgecrust/mantle structures, particularly in triassic basins, account for structural/thermal conditions and provide new tecto-thermal informationon the evolution of the Saharan platform.

## II 2. Methology :

### II.1 Model conceptualisation :

In this study, a comprehensive compilation of multidisciplinary data (Fig. 2) was conducted to develop a conceptual model aimed at providing insights into the thermal composition and associated geodynamic processes within the lithosphere-asthenosphere layers. The multi-scale data used as input during the model-building process included geophysical data such as gravity, magnetic, topography, elevation, geoidal height, and heat flow, along with petrological data providing information on the chemical composition of the sub-continental lithospheric mantle.

Isostatic gravity data was utilized to derive the Moho depth, while magnetic data aided in deriving information on the magnetic basement and geothermal gradient. Additionally, potential field data offered insights into crustal lithospheric geometry, as well as tectonic and structural constraints used in developing the initial model.

#### II.1.1Geophysical data :

The gravimetric and topographic datasets utilized in this study were sourced from the global gravity version 28.1 model, incorporating the EMG2008 global model, as well as data from Topex/Poseidon, Jason-1 satellite altimetry, and Cryosat-2 Radar satellite altimetry/gravity satellite information. These datasets were gridded with a resolution of 1 arc-minute. Detailed information about the data sources can be found in publications by (Smith and Sandwell 1997), (Garcia 2007), (Fullea 2008), (Pavlis 2012), and (Sandwell 2013 & 2014). Additionally, the data can be accessed from https://topex.ucsd.edu/cgi-bin/get_data.cgi.

Geoid data was obtained from ICGEM EIGN 6C4 (Foerste et al., 2014) and can be downloaded from http://icgem.gfzpotsdam.de/calcgrid?modeltype=longtime&modelid=7fd8fe44aa1518cd79ca84300aef4b41ddb2364aef9e82b7cdaabdb60a9053f1. Shallow noise effects on the data were corrected by applying the upward continuation filter, with a variable upward distance depending on the data type. Specifically, a 2.5 km filter was used for free-air data, while a 5 km filter was applied for topographic data. Topographic correction was performed using the ETOPO1 digital elevation model (Amante and Eakins, 2009).

Heat flow information was obtained from Bottom Hole Temperature (BHT) and Drill Stem Test (DST) measurements, while calculated heat flow data was derived from interpretations of EMAG3 V2 magnetic data and the application of the centroid method (Bhattacharyya and Leu, 1975; Tanaka, 1999). These methods were adapted from previous work by (Melouah 2021

### II.1.2Tectonic and structural data

The structural information utilized in this study was derived from interpretations of residual magnetic maps from previous works in the area, as described by (Melouah2021). The EMAG3 V2 magnetic data underwent reduction to the magnetic pole by applying an inclination of 44.93° and declination of 1.23°. Subsequently, the data was re-gridded to a resolution of 2.5×2.5 km using the kriging method. Additional details on the data treatments can be found in (Melouah 2021).

### II.1.3Composition of crust and lithospheric mantle :

The key compositions of the crust and lithospheric mantle layers (Table 1) were assessed based on xenoliths within the Hoggar basin and reports from related lithospheric domains (Griffin 2009 Kourim 2014). However, it's important to note that the lithospheric mantle composition is influenced by the age of the crust overlaying it. Studies indicate that the most depleted sections of the lithospheric mantle are found in Archean and Proterozoic cratons (Zheng 2001; O'Reilly 2001; Griffin and O'Reilly, 2007; Tunini 2016). Elements such as Fe, Ca, and Al, which are chemical constituents of the lithospheric mantle, directly impact its geophysical properties. Low Fe content implies low density and high seismic velocity, while medium to high Al content suggests high seismic velocity.

Geochemical data from Iherzolite analyses in the Archean sub-continental lithospheric mantle and the Tafadest-Iskel terrane in central Hoggar, as reported by Griffin et al. (2008) and Kourim et al. (2014) respectively, revealed similarities in xenolith chemical composition (Table 1). However, in this study, central Hoggar xenolith data were only used as a comparative reference and not incorporated into the model construction due to the geological complexity of the Hoggar terrane, which could potentially influence model outcomes.

The sub-continental lithospheric mantle (SCLM) exhibits high compositional heterogeneity and is influenced by the thermo-tectonic age of the overlying crust (Sobh 2020). The SCLM composition is characterized by a system of major oxides (Table 1), CFMAS (Griffin 2008) This thick section of depleted cratonic SCLM is buoyant and rigid relative to the convective mantle (Poudjom-Djomani2001; Afonso and Ranally 2004), providing resistance during major tectonic events. Metasomatism processes decrease the viscosity and buoyancy of the SCLM, resulting in vertical compositional gradients (Griffin 2008). Below approximately 10-20 km depth, the SCLM becomes more fertile and is bounded by an intense zone of melt (O'Reilly and Griffin, 2006; Afonso 2008; Fullea 2009). Despite this, the SCLM remains buoyant relative to the asthenosphere (O'Reilly 2001; Griffin 2008).

| Composition | Central Hoggar Lower Crust (Leyreloup et al., 1982) | Mantle (Griffin et al., 2009) | Hoggar Iherzolite (Kourim et al., 2014) | |
|---|---|---|---|---|
| | | | Tafadest | Iskel |
| $SiO_2$ | 53.18 | 44.76 | 44.88 | 45.34 |
| $Al_2O_3$ | 16.72 | 3.52 | 3.08 | 3.17 |
| FeO | 9.47 | 8.05 | 8.76 | 8.7 |
| MgO | 5.96 | 40.04 | 39.82 | 39.62 |
| CaO | 8.06 | 3.12 | 2.94 | 2.86 |
| $Na_2O$ | 3.06 | 0.24 | 0.15 | 0.08 |

**[Table1] :**Average values of the crustal and lithospheric mantle oxides composition used in building the initial model

## II.2Model structure :

### II.2.1 LitMod-2D modeling and assumption :

Lithospheric modeling in 2D (LitMod-2D) is a finite element code designed to integrate geophysical and petrological information to analyze the thermal, seismological, density variations, and compositional characteristics of the lithosphere and uppermost mantle layer. This code facilitates the evaluation of the 2D distribution of seismic velocity, density, and temperature down to a depth of 400 km. Detailed information on LitMod-2D can be found in (Afonso 2008).

Mantle anelasticity effects were incorporated into the model based on oscillatory periods, grain size, and pressure-temperature (P-T) conditions available in Afonso et al. (2008). The heat transport equation utilized a steady-state finite element method with boundary conditions set at the surface and the Lithosphere-Asthenosphere Boundary (LAB), with temperatures of 0°C and 1300°C respectively. It was assumed that there was no lateral flow of heat across the model boundary. This assumption of steady-state heat transfer within the Saharan platform is supported by the relative stability of the crust in the region. Furthermore, due to the sparse distribution of Bottom Hole Temperature (BHT) and Drill Stem Test (DST) measured heat flow data, it was challenging to account for volumetric thermal effects (Jaupart1983 Petitjean 2006; Stephenson 2009 Melouah 2021).

A thermal buffer zone of 40 m was applied at the bottom of the LAB, with a base temperature of 1400°C. This buffer zone serves to prevent unrealistic discontinuities between the

lithosphere, characterized by a conductive thermal gradient, and the asthenosphere, which exhibits an adiabatic thermal gradient. Below the thermal buffer zone, temperature gradients were restricted to ≤ 0.35 to ≤ 0.50 to avoid modification of the base temperature, set at 1520°C/km at a depth of 400 km (Afonso 2008).

**II.2.2Moho depth calculation :**

Several empirical equations have been used in literature to evaluate the Moho depth. Over the years, researchers have applied different approaches in an attempt to evaluate the geometry of density interface that delineate the Moho discontinuity (Woollard, 1959Riad1981 Chakraborty and Agarwal 1992Lefort and Awarwal 2000). In this study, the (Woollard1959) formula that relates the depth to Moho ($Z_{moho}$) and regional gravity anomaly (g) was utilized. Hence, the Mohodepthcanbeexpressed as

$$Z_{moho} = 32 - (0.08 \times g) \quad (1)$$

The Moho calculation was performed by employing the isostatic gravity data acquired from the Bureau Gravimetric International. The airy compensation applied is 30 km for crustal thickness, and density correction of 2.67 g/cm$^3$ was applied. The isostatic gravity was separated into regional and residual components and only the regional component was applied in Eq. 1.

**II.2.3 Lithosphere-asthenosphere boundary (LAB) calculation :**

(Fullea2007) approach that relates topography and geoid deformation was adopted during the lithosphere-asthenosphere boundary calculations. (Lachenbruch and Morgan 1990) described the elevation (*E*) under the assumption of local isostasy as

$$E = \frac{\rho_a - \rho_L}{\rho_a} \cdot (L - L_0) \quad , (E > 0) \quad (2)$$

$$E = \frac{\rho_a}{(\rho_a - \rho_W)} \left[ \frac{\rho_a - \rho_L}{\rho_a} \cdot (L - L_0) \right] \quad , (E < 0) \quad (3)$$

where *L* is thickness of the lithosphere, asthenospheric density $\rho_a = 3.24\ \mathrm{g/cm^3}$, the depth of free asthenospheric level $L_0 = 2320$ m, and $\rho_L$ is lithospheric average density (Fullea2007). For a flat-earth model, the vertical density distribution arising from the dipolar moment underneath the observation points is proportional to the geoid anomaly (*N*) (Ockendon and Turcotte, 1977Fullea 2007).

$$N = -\frac{2\pi G}{g} \int_{LC} Z \cdot \rho(z) dz + N_0 \quad (4)$$

where $G$ represents the gravitational constant, $g$ is the terrestrial acceleration of gravity, $\Delta\rho$represents the density contrast, $N_0$ is a constant considered to be the reference datum required to condition the level 0 of the geoid anomalies. More so, in the preliminary model, constant crustal and mantle densities, i.e., 2.7 and 3.2 g/cm$^3$ respectively, were used. The LAB depth can be obtained by combining empirical equations from (Fullea2007) as :

$$Z_L = \frac{1}{\rho_a - \rho_c}\left(K + \sqrt{\frac{\rho_m - \rho_c}{\rho_m - \rho_a}(K^2 - (\rho_a - \rho_c)\left[E^2(\rho_w - \rho_c) + Z_{\max}{}^2\rho_a + (N - N_0)\frac{g}{\pi G}\right]}\right) \quad (5)$$

$$K = \rho_a L_0 + E(\rho_c - \rho_w) \quad (6)$$

$$N_{0c}(E,N) = \frac{\pi G}{g}\left[E(\rho_w - \rho_c) + Z^2\frac{K^2}{\rho_a - \rho_c}\right] + N \quad (7)$$

**II.2.4 Lithospheric density calculation:**

Hence, the density of lithospheric mantle can be expressed as:

$$\rho_{Lm} = \rho_{m_0}\left[1 - \frac{\alpha(T_{Moho} + T_{LAB})}{2}\right] \quad (8)$$

where$\rho_{Lm}$ is *in situ* mean lithospheric density, average density derived from standard penetration test $\rho_{m_0} = 3.38\,\mathrm{g/cm^3}$ of the upper mantle evaluated from mantle Phanerozoic xenoliths (Poudjom-Djomaniet al., 2001; Xia et al., 2020), coefficient of thermal expansion $\alpha = 3.5 \times 10^{-5}K^{-1}$, $T_{moho}$ and $T_{LAB}$ = 1300°C represents the Moho and LAB temperatures respectively. Also, theasthenospheric mantle density can be estimated using (Xia 2020) empirical model.

$$\rho_{AM} = \rho_{m_0}(1 - \alpha T_{LAB}) \quad (9)$$

**II.2.5 Calculation of lithospheric mantle temperature:**

$T_{LM}$is the mean lithospheric mantle temperature equivalent to the average $T_{moho}$and $T_{LAB}$(Zhang 2020).

$$T_{LM} = \frac{(T_{moho} + T_{LAB})}{2} \quad (10)$$

The Moho temperature is influenced bylithospheric mantle thickness ($Z_{LAB}$)and the geothermal gradient *dT/dz* (Zhang 2019; 2020.(Xia 2020).

$$T_{moho} = \left[T_{LAB} - \frac{dT}{dz}(Z_{LAB} - Z_{moho})\right] \quad (11)$$

$$dT/dz = 537 \cdot (Z_{LAB})^{-0.88} \quad (12)$$

**II.2.6 Calculation of lithospheric mantle residual gravity anomaly :**

The residual gravity anomaly arising from the lithospheric mantle was deduced by subtracting the crustal gravity ($\Delta g_{crust}$)effect due to sediments and the Moho, and the LAB influence($\Delta g_{LAB}$) from free-air-gravity anomaly($\Delta g_{obs}$), and adding the reference gravity model ($\Delta g_{ref}$).

$$\Delta g_{mg} = \Delta g_{obs} - \Delta g_{crust} - \Delta g_{LAB} + \Delta g_{ref} \quad (13)$$

The terms $\Delta g_{crust}$and $\Delta g_{LAB}$of Eq. 13were calculated using the Bouguer plate correction

$$\Delta g = 2\pi G\rho h \quad (14)$$

where the universal gravitational constant is represented as *G*, layer thickness and density as *h* and$\rho$respectively.

**II.3Model outputs**

The 2D numerical modeling of density, temperature, and seismic wave velocities, including P and S waves, was achieved using the LitMod-2D code, as described in detail This method utilizes petrophysical and mineral physics principles to estimate relevant thermo-physical properties of the upper mantle ( Tašárová, 2009). Density variations were evaluated using iterative fourth-order Birch-Murnaghan equations, and bulk rock densities were determined based on the arithmetic average of individual phases weighted by their volumetric fraction (Tašárová, 2009).

Seismic wave velocities were calculated based on the elastic moduli of individual end-member minerals and the bulk rock density at the relevant temperature and pressure conditions To adequately represent the distributions of P- and S-wave velocities, density, and temperature, two transects were established. Profile A-A' was oriented NW-SE of the Saharan platform, while the B-B' transect was oriented along the NE-SW direction.

One advantage of this modeling method is that it provides better lateral and vertical control of observable geophysical data such as free-air gravity, geoid, topography, and petrological data used to produce the seismic velocity, density, and thermal distribution models of the upper mantle. The simultaneous and self-consistent fitting of long-wavelength components of geophysical data and petrological data reduces the uncertainties associated with fitting these observed data independently or in pairs on a stand-alone basis

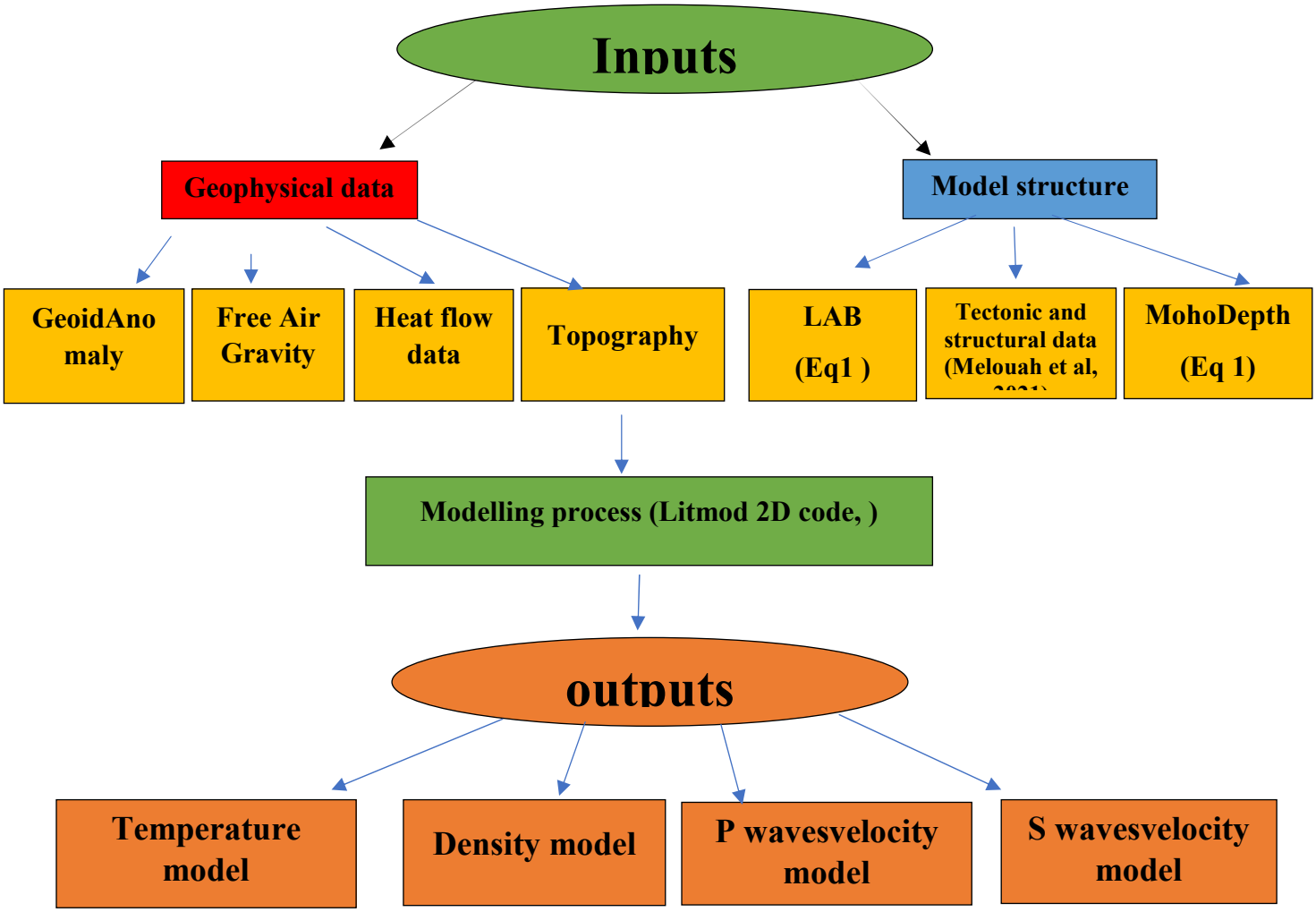


**[Fig.02]:** the schem of the modeling process for the saharan platform , using multidisiplinary data sets

# Chapitre III :Results and Discussion

## III.Results and discussion :

### III.1Delineation of crustal structures :

The total magnetic anomaly in formation was reduced to the magnetic pole, after applying inclination and declination of 44.93° and 1.23° respectively, and was later upward continued to 1500 m (supplementary materials), to enhance deep structures. The residual magnetic map (Fig.3) indicates values that range from -40 to 70 nT. The anomaly distribution is controlled by the underlying rock magnetization and crustal architecture. The high anomalies or positive axes represent the HassiMessaoud-AmguidEl-Biod horst, Rhoud El Baguel-HassiTouareg anticline, Djamaa-Touggourt saddleback structures and Tilhemt anticline. More so, the low anomalies or negative axes represent Melghigh trough, Dorbangraben, Ghadames and Oued Mya depressions.

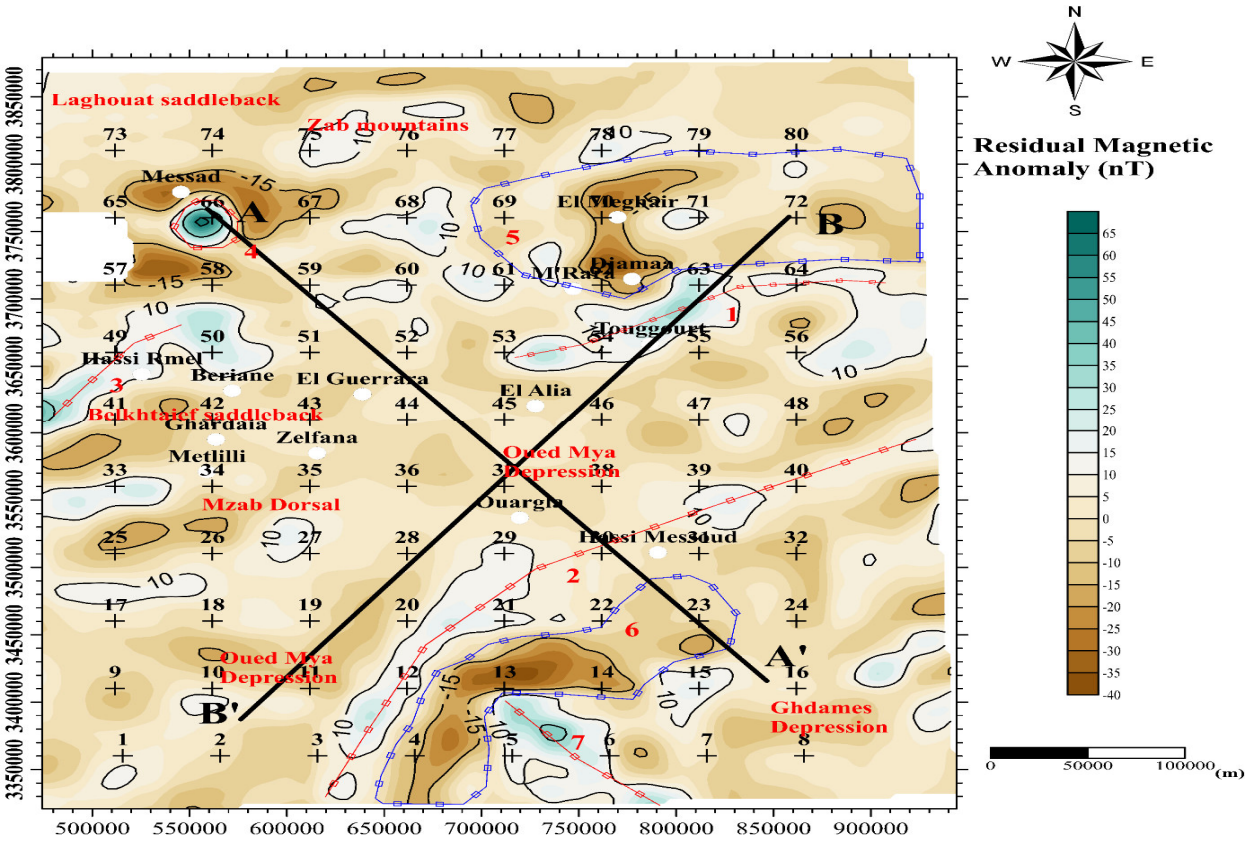


**[Fig. 03]:**Residual magnetic map showing interpreted structural components of the Saharan platform. The A-A' and B-B' transects represent the profiles along which the LitMod-2D code was applied during the modeling process. The numbers 1-7 were used to identify the interpreted structural units as follows; 1. Saddleback structures of Djamaa-Touggourt, 2. HassiMessaoud-Amguid horst, 3. Anticlinal structure of Tilhemt, 4. Unknown circular structure, 5. Melghigh trough, 6. DorbanGraben, 7. Anticline of Rhoud El Baguel-HassiTouareg

The transformation of the magnetic spectra enabled the calculation of the Curie isotherm depth (Aydemir 2019). The outcome of the centroid analysis of the magnetic data (Bilim 2021Bilim 2021) that was used to image the heat flow distribution are presented in Fig.4b. Heat flow distribution lie between 65 to 122 mW/m$^2$ and on average 89 mW/m$^2$. The highest records were encountered along the HassiMessaoud-AmguidEl-Biod horst, Rehabi-Berriane-Djerba structural axis and towards the western limit of M'zab Dorsal. Conversely, lowest values that appeared to be associated with structural depressions and grabens were observed around the Melghigh trough and Oued Mya depression and Dorbangraben. Previous studies suggested different values of Curie depth (33 to 43 km) within the region, and estimated heat flow to be 68 mW/m$^2$ with window size of 1000×1000 km (Elbarbary 2022). The correlation with measured heat flow (e.g. DST and BHT) indicates strong similarities (Fig. 4). Several factors were observed to have influenced heat transfer from deep sources to the surface. These include thermal conductivity of sedimentary cover and intensity of fault network.

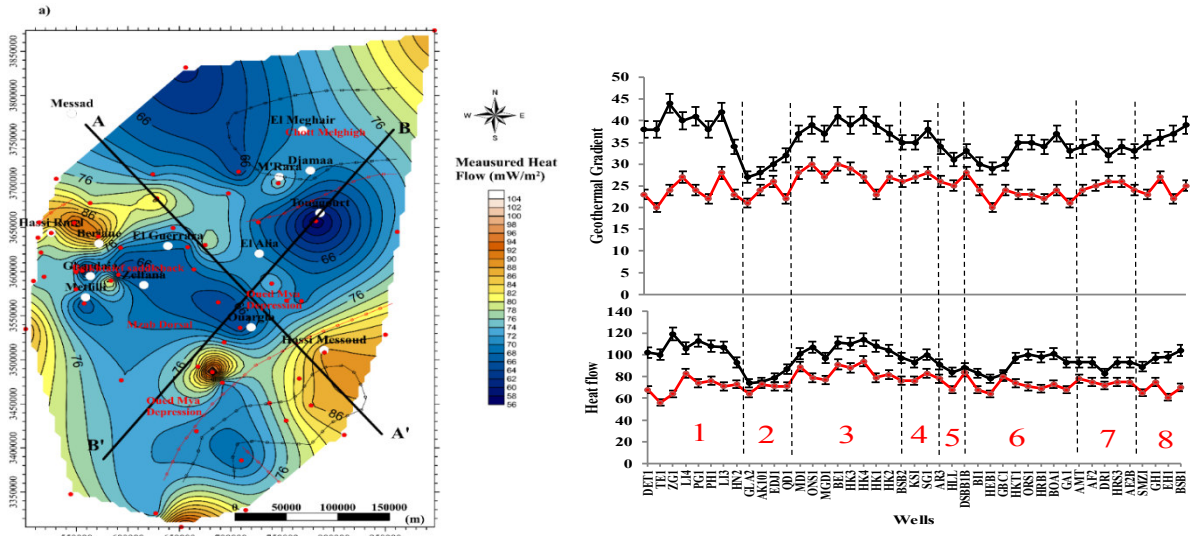


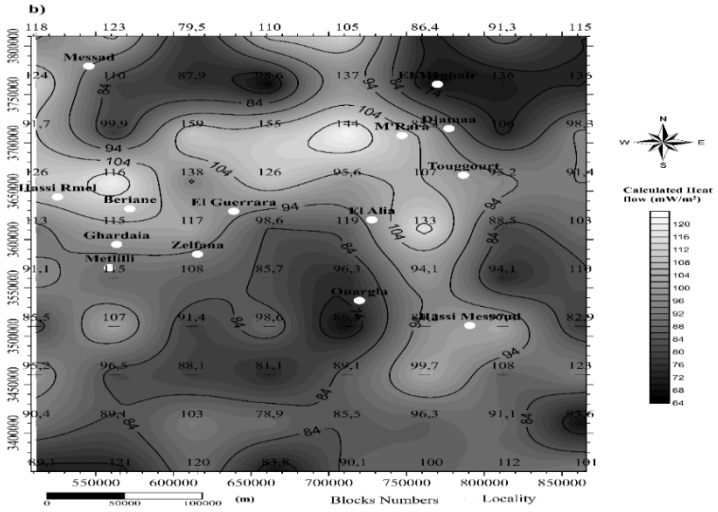

**[Fig.04]:**(a) Heat flow maps displaying measured values obtained from Bottom Hole Temperature (BHT) and Drill Stem Test (DST) conducted in petroleum wells, covering depth intervals ranging from 700 to 4400 meters.
(b) Heat flow maps presenting calculated values derived from the application of the centroid method on aeromagnetic data.
(c) Comparative plots illustrating estimated and measured heat flow, as well as geothermal gradient, within each of the interpreted geologic structures numbered 1-7 in Fig. 2. The estimated values from our study are represented by black dotted curves, while the measured values from BHT and DST tests are depicted by red dotted curves

## III.2Moho and LAB depth :

The crustal structures depicted in Fig. 5a and b reveal significant variations in the depth to the crust-mantle interface across the study area. In the eastern segment of the Melghigh basin, located towards the Saharan Atlas, the observed depth to the crust-mantle interface exceeds 36 km. Moving towards the northwestern flank beneath the M'zab dorsal, the Moho depth ranges between approximately 30 to 32 km. In contrast, towards the center and southeastern limits, the Moho appears relatively flat.
The temperature of the Moho varies within the range of 415 to 498°C across the study area. The lowest temperatures are encountered within the northwestern parts of the M'zab valley, while the highest values are found towards the southeastern axis. Notably, isotherms ranging from 465 to 490°C intersect the axis of Touggourt-Djamaa-El M'Ghair, which is considered a geothermal potential area within the Eastern Algerian Sahara (Table 2).

**[Table 2] :**
Summary of temperature values of known geologic structure in the Saharan platform

| Profile | Structure | Temperature values °C |
|---|---|---|
| A-A' | HassiMassaoud-AmguidEl-Biodhorst | 483-486 |
| | Dorban Graben | 483-489 |
| | Mzab Dorsal | 457-470 |
| | Rehabi-Beriane-Djerba structure | 440-450 |
| B-B' | Melghightrough | 483-486 |
| | Oued Myadepression | 467-469<br>477-479 |
| | Touggourt Djama structure | 474-475 |
| | Allalvoute or Arak Idjerane horst | 474.5-476.5 |

Generally, the LAB depth increased with thermo-tectonic age due to conductive cooling (Liu 2021). The observed result (Fig. 6a) indicates that the northwestern limit is thicker (~199 to 222 km), while thinner lithosphere was observed within the southeastern limit (~177 to 187 km).

## III.3Interpretation of gravity residual signature by stripping :

The Moho and Lithosphere-Asthenosphere Boundary (LAB) grids were utilized to compute the lithospheric mantle and asthenospheric residual gravity anomaly. Due to a lack of studies

and knowledge regarding thermal lithospheric properties in the Algerian Sahara, a mean value for the standard pressure-temperature (P-T) density of fertile mantle ($\rho_{M0} = 3.38$ g/cm³) was adopted (Poudjom-Djomani 2001 /Fullea 2009; Xia 2020).

The results indicate that the calculated in-situ average densities for the lithospheric mantle and asthenosphere range between 3.273 g/cm³ and 3.278 g/cm³, respectively (see Fig. 6b).

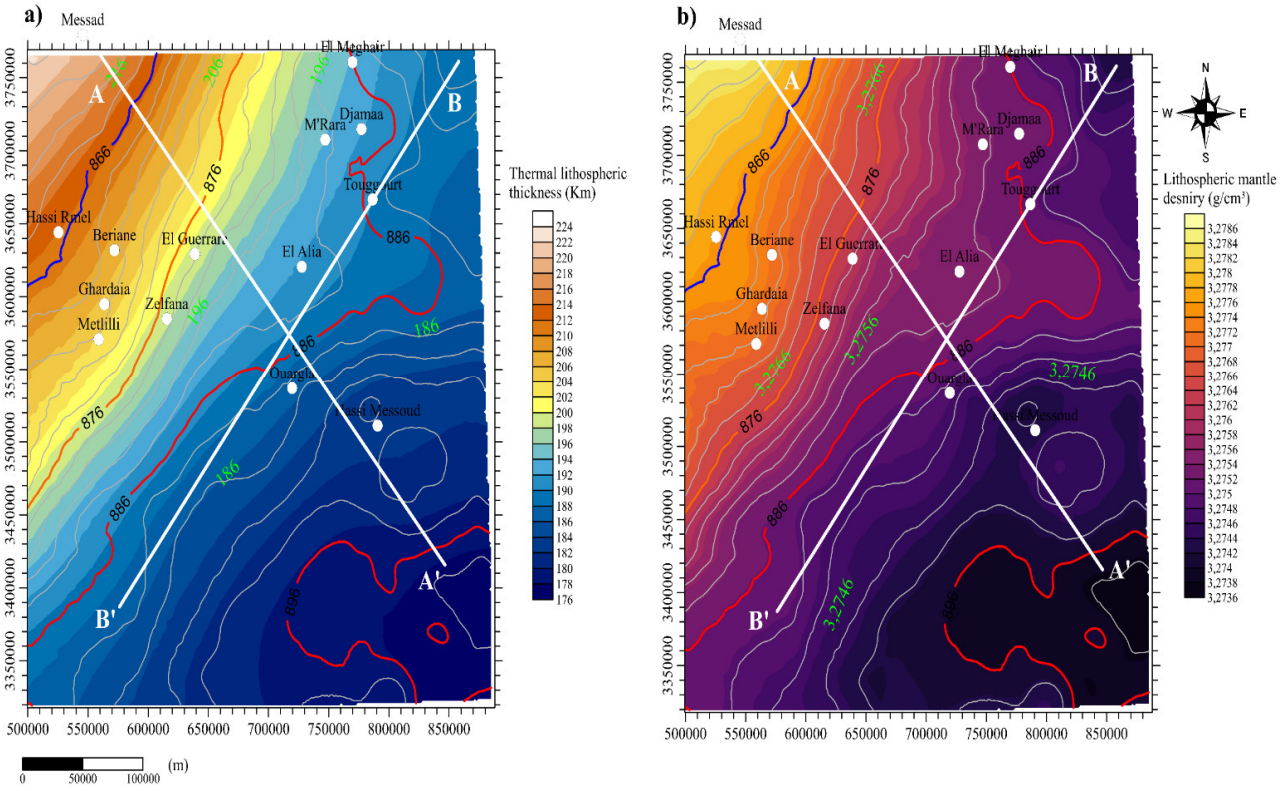


**[Fig.05]:**(a) A lithospheric thickness map depicting the thickness of the lithospheric mantle and its associated temperature.

(b) A distribution map showcasing the density of the lithospheric mantle overlaid onto the estimated layer temperature

The residual lithospheric mantle gravity was derived by subtracting the gravitational effects attributed to the crust (as shown in Fig. 7a) and the Lithosphere-Asthenosphere Boundary (LAB) (as shown in Fig. 7b) from the free-air gravity anomaly. The crust-LAB gravity signature was obtained by applying the Bouguer plate correction. Studies and Shulgin and (Artemiev2019) have suggested that the effects of uniform density of the crust and sharp changes in Moho and LAB depth can be neglected as they do not significantly impact the final solution.

The gravity anomaly is notably influenced by the low to moderate density of sediments and the architecture of the Moho (as depicted in Fig. 7a). The gravitational effect attributed to the crust from the surface to the Moho varies from 34 to 43 mGal and exhibits significant similarity with the residual magnetic anomaly map (as shown in Fig. 3). The uplift of the basement contributes to the distribution of surface gravity anomalies, with the Melghigh trough characterized by mean gravity values of approximately ~42 mGal, while the HassiMessaoud-Amguid El-Biod horst ranges between 39 and 41 mGal. Lower values were encountered towards the northwest of the M'zab dorsal.

It's important to note that the signature of subsurface structures may appear slightly exaggerated in some zones due to the paucity of data (such as density diagraphy) and possibly the assumption of a uniform crustal density (i.e., 2.7 g/cm³).

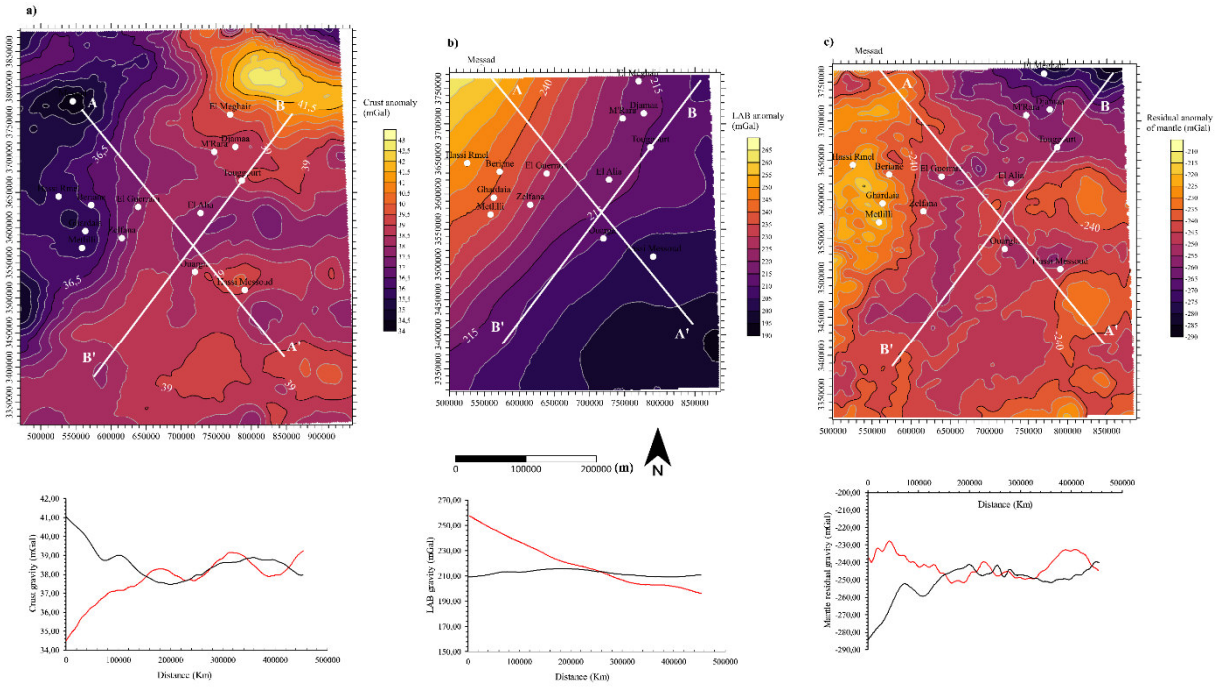


**[Fig.06]** :Application of stripping to the free-air gravity data a) calculated crust gravity anomaly using Bouguer plate formula and comparaison between the results alongA-A' and B-B' transects. b) the generated gravity anomaly in the LAB layer and compared signal along A-A' and B-B' profiles c) the obtined residual anomaly of the mantle and comparative anomaly along A-A' and B-B' transects. Red lines represent the variation in parameters along A-A' transect while the black line is the variation of parameters along B-B' transect

## III.4Lithosphere-asthenosphere model :

The modeling results from the LitMod-2D code indicate a thick lithospheric mantle along the two transects A-A' and B-B' (refer to Fig. 8), with the Lithosphere-Asthenosphere Boundary (LAB) extending to depths of approximately 200 km. Along profile A-A' oriented NW–SE,

the LAB depth increases from 176 to 225 km beneath the Ghadames-Berkine basin. The crustal thickness, based on the modeling results, remains constant, except for some evidence of deformation along the center of the profile corresponding to structural depression. Along section B-B', the LAB depth reaches around 190 km, with slight deformation observed along the center of the profile corresponding to the Oued Mya depression, while an uplift is noted towards the southeastern segment under the AllalVoute limit or the Idjerane horst. Similarly, the variation in Moho depth was insignificant, as the Moho appeared relatively flat, reaching depths of around 37 km.

A comparison between the calculated results using empirical relationships by (Woollard 1959) for Moho depth, for LAB estimation, and the LitMod-2D modeling calculator shows significant differences, especially on profile B-B', where the difference in Moho depth exceeded 10 km. This discrepancy between the various estimates can be attributed to the empirical approach employed.

Studies in other regions provide additional context. For example, modeling results in the Northern China craton using a multi-geophysical, geochemical, and thermal approach showed estimated LAB depths between 90 and 180 km, Moho temperatures between 400 and 1000°C, and lithospheric mantle densities between 3.27 and 3.43 g/cm³ (Zhang 2020). Similarly, studies within the Middle East characterized crustal thickness ranging from 8 to 60 km, with thick crust located along the north of the Zagros fault towards the Eurasian plate and thin crust found within the Indian plate, Gulf of Aden, Red Sea, Black Sea, and Eastern Mediterranean Sea (Kaban 2017).

In Western Gondwana, Moho depths estimated using S-receivers ranged from 15 to 50 km, while LAB depths reached 50 to 120 km in non-cratonic zones Evaluations of crust and uppermost mantle layer thicknesses in the Gibraltar arc system and Moroccan Anti-Atlas mountain suggested Moho depths between 2 and 46 km and LAB depths between 50 and 200 km

Recent research in the Saharan Metacraton and proximity zones revealed Moho depths between 35 and 39 km in the Saharan platform, shallower along the western African rift system, but deeper within the central African rift system (~37 to 40 km) (Maddaloni 2021). The LAB was found to be deeper in the eastern limit of the Saharan platform (170-200 km) and in Al Kufrahcratonic remnants, with shallower LAB depths encountered in the Cameroun volcanic line and Tibesti massif (Sobh 2020).

## III.5Seismic wave velocity model :

Modeling results indicate that the velocity of the P-waves in the Saharan platform (Fig.8a,e) increases vertically from crustal surface towards the mantle. The values range from <8.15 to 8.55 km/s. The crust is characterized by low values, while high values were encountered within the upper mantle layer. Within the area, structures of the upper mantle were relatively homogeneous. The S-waves in profiles A-A' and B-B' (Fig,8b,f) range from 4.45 - 4.50 km/s. Variation in wave velocities were controlled by the composition and deformation of the transitional layers. Similar studies in the Namibian volcanic margin showed that the velocity ofP-waves ranged from 7.7 to 8.4 km/s, while S-wave velocity ranged from 4.2 to 4.8 km/s (Fernandez et al., 2010).

## III.6Temperature and density models :

To facilitate the understanding of vertical changes in thermo–structural signature, two cross-sections (i.e., A-A' and B-B') of density and temperature as observed in Fig. 8c,g were selected. The temperature increased gradually downwards from the upper crust towards the mantle. Table 3 illustrates the temperature of the crust, lithospheric mantle and asthenosphere along the cross-sections. The inversion result shows that the Curie isotherm corresponding to 580°C (Chopping and Kennett, 2015) was observed at ~60 to70 km depth in profile A-A'. Conversely, profile B-B', considered to be flat was at 60 km depthdemonstrated that the region has high potential for geothermal energy production, and estimated the Curie isotherm depth at 12.8 to 21.0 km using the centroid method applied to magnetic data. (Elbarbar2022) gave a different approximation and suggested that the Curie isotherm is 36 to 45 km deep in the Algerian Saharan platform.

**{Table 3**Comparative studies showing: crust depth, LAB depth, of P- and S-wave velocities,

| Layer | Depth (km) | $V_P$wave (km/s) | $V_S$ wave (km/s) | Density (km/s) | Temperature (°C) | Source |
|---|---|---|---|---|---|---|
| Crust (includingsediments) | 35-40 | - | 3.40-3.70 | - | - | Pasyanos and Walter (2002) |
| Lithosphericmantle | - | - | 4.45-4.65 | - | - | |
| Asthenosphericmantle | - | - | - | - | - | |
| Crust (includingsediments) | 36-38 | - | - | - | - | Globig et al. (2016) |
| Lithosphericmantle | 180-200 | - | - | - | - | |
| Asthenosphericmantle | - | - | - | - | - | |
| Crust (includingsediments) | 30-40 | - | - | 2750-2850 | - | LithRef18 (Afonso et al., 2019) |
| Lithosphericmantle | 160-200 | - | - | 3470-3490 | - | |
| Asthenosphericmantle | - | - | - | 3460-3475 | - | |
| Crust (includingsediments) | 36-39 | - | 4.50-4.80 | 3315-3330 | 350-450 | Sobh et al. (2020) |
| Lithosphericmantle | 170-200 | - | 4.40-4.55 | 3425-3430 | 1350-1375 | |
| Asthenosphericmantle | - | - | - | - | >1400 | |
| Crust (includingsediments) | 35-40 | <8.15-8.20 | 4.45-4.50 | 2750-2900 | ≤ 400 | Present study |
| Lithosphericmantle | 175-220 | 8.20-8.3 | 4.50-4.70 | 3000-3400 | 400-1250 | |
| Asthenosphericmantle | - | 8.30-8.55 | 4.50-4.65 | 3400-3600 | >1250 | |

temperatures and densities within the Saharan platform from this study and international modelsux

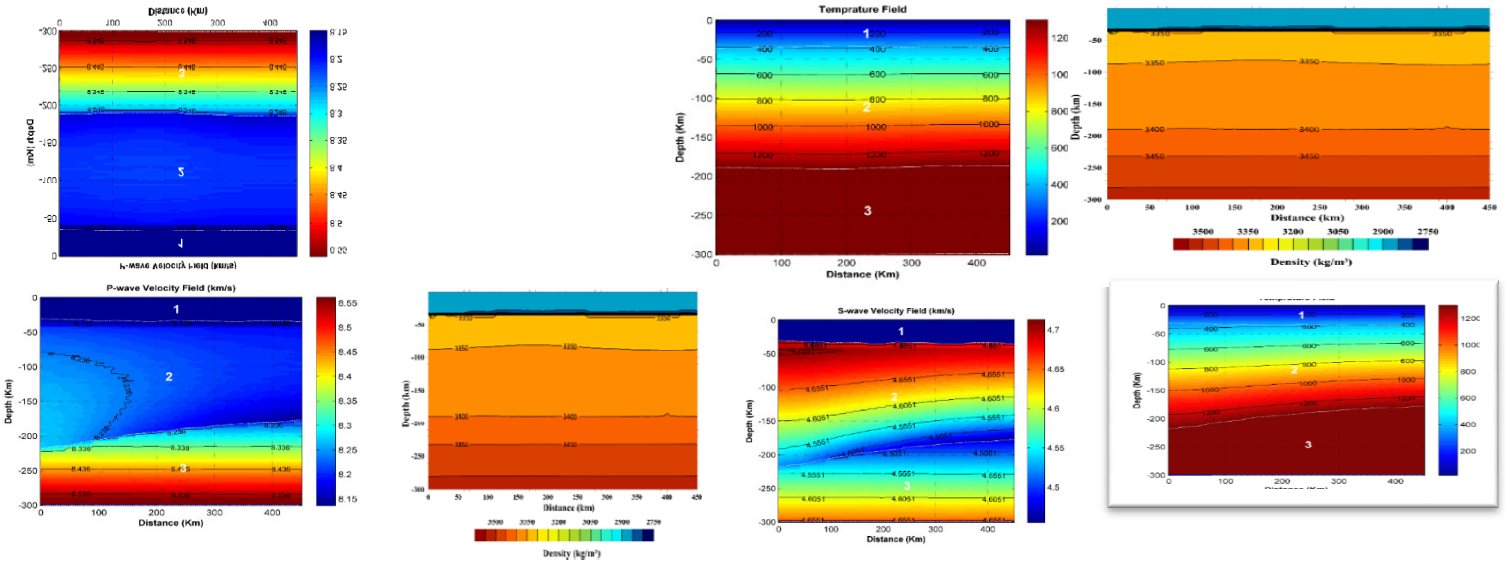


**[Fig.07]:** Results of the physical property modeling using LitMod-2D code, a) P-wave velocity along A-A' transect, b) S-wave velocity along A-A' transect, c) temperature distribution along A-A' transect, d) density distribution along A-A' transect, e) P-wave velocity along B-B' transect, f) S-wave velocity along B-B' transect, g) temperature distribution along B-B' transect and, h) density distribution along B-B' transect. The numbers 1, 2 and 3 represents crustal thickness, lithospheric boundary, and asthenosphere

The estimated temperature within the Mohorovicic discontinuity and lower mantle boundary were compared using two different techniques. The estimation of Moho temperature using Eqs 11 and 12 shows values between 420 and 495°C. Also, the inversion results using LitMod-2D code show estimates of the Moho temperature to range from 350 to 400°C in the cross section A-A' while B-B' profile which was flat show uniform temperature of 400°C. For the lithospheric mantle, applying the empirical relation in Eq. 10, the estimated temperature shows variability from 858°C to 898°C, while estimates of 400 to > 1200°C were achieved based on LitMod-2D inversion results. The density variation is controlled by the petrographic and geochemical compositions as well as the thermodynamic reactions that occurred during melting and convection mechanism. Generally, density increased from the upper crust (i.e. 2.75 g/cm$^3$) towards the mantle where it attained values > 3.50 g/cm$^3$ (Fig.8d,h). On the other hand, calculations of the density values within the lithospheric mantle

using Eq. (8) shows a low-density distribution with values that range between 3.27 and 3.28 g/cm$^3$.

.The main contribution of this research is to estimate the thermal structure, density, and temperature architecture of the crust and upper mantle of the eastern Triassic province within the Algerian Saharan platform (refer to Fig. 9). Regional studies indicate that Archean cratons are three times more productive in radiogenic heat flow than post-Archean and Proterozoic crusts, suggesting differences in mantle composition beneath them (Rudnick 1998/ Artemieva and Mooney, 2001/ Artemieva and Vinnik 2016).

The Saharan platform is in isostatic equilibrium, with lithospheric roots compensated by adjacent structures of different compositions such as the Saharan metacraton, Hoggar shield, and West African Craton (Perron, 2019/ Takherist* 1991). Reference to similar studies in zones adjacent to the Saharan platform with potentially different geological histories and thermal events has been made due to a lack of studies interpreting the relationship between the lithospheric and asthenospheric layers in the area. Crustal deformations have been interpreted based on the presence of thermo-structural events such as the aborted rift series in the Ougarta range and the subduction process in proximity to the Reggane basin (Caby 1987/ Lamali 2013/ Melouah 2021).

Studies within the Saharan metacraton have categorized the mantle lithosphere based on thickness, density, and seismic velocities, suggesting that the Al Kufrah remnant craton is dissimilar to the main Saharan metacraton and may have originated from the partial metacratonization of the ancestral Saharan metacraton during Neoproterozoic collisional delamination events (Sobh 2020).

In the Hoggar shield to the south of the Saharan platform, deformation in the lithospheric mantle has been suggested to result from lithospheric delamination within the Pan-African mega-shear zone or along the metacratonic margin (Liégeois 2005/Jiang 2022) Xenoliths from the South Hoggar representing fragments from the lithospheric mantle located beneath the shear zone show substantial variations in chemical composition, temperatures, and microstructural deformations, interpreted as the occurrence of vein-conduits and metasomatic trans-lithospheric melts of the Cenozoic (Kourim 2014).

The results of this study reflect large-scale geologic events in the area, with seismic velocities, gravity anomalies, and the geoid reflecting current geologic structures, while temperature, density, and heat flow distribution models relate to events over long geologic periods that characterize the Saharan platform.

**5-Moho model validation and discrepancies**

To facilitate the evaluation of the accuracy of our gravimetric evaluations, the estimated Moho depth based on gravimetric model was compared with Moho depth derived from CRUST 1.0, i.e., based on seismic data (Fig. 10). The resolution of CRUST 1.0 Moho depth model is 1×1 degrees and was re-gridded based on the resolution of the gravimetric Moho depth map. The gravimetric Moho depth shows strong similarity with the seismic derived Moho depth with minimal misfits, i.e. mean and standard deviation were of the order 1.95 and 1.45 km respectively (Fig. 10f). The misfits between models can be accredited to the missing details in the seismic Moho, indicated by smooth configuration over large areas (Van der Meijde 2015; Globig 2016/Shehata and Mizunaga 2022). The constant Moho configuration between El Guerrara and El Meghair and between Ouargla and Touggourt along the cross-section BB' (Fig. 9a,b,d,e) are indications of missing geologic information. Additionally, the gravimetric Moho shows good correlation with dominant regional structures. However, the locations of these misfits aligned with locations of these dominant structures (e.g. Messad uplift and Melghigh trough) and were validated by magnetic signatures within these locations. Conversely, these structures were missing in the seismic Moho depth derived from CRUST 1.0. Previous Moho depth estimates of 35 and ~38 km observed by (Buness1992) and Sandvol et al. (1998) within the Saharan platform and Hoggar respectively are within the range of 30 and 38 km of our study. Petroleum studies have reported dominant structures, i.e., the basement structural uplift within Messad and elsewhere the Melghigh trough (Takherist 1991), which were absent in the seismic Moho configuration. These structures were observed in the gravimetric Moho as undulations which provide additional validation. More so, the difference in Moho depth between the models (i.e., ~5.3 km) observed within the Messad uplift is indicative of the missing information in CRUST 1.0 model which validates the effectiveness of the gravimetric model. The estimate from this study provides more precise Moho configuration and structural information that can be used to update existing seismic based Moho model within the Saharan platform. It can also be used as reference model for lithospheric structural mapping to enhance the understanding of the geodynamic characteristics of the area.

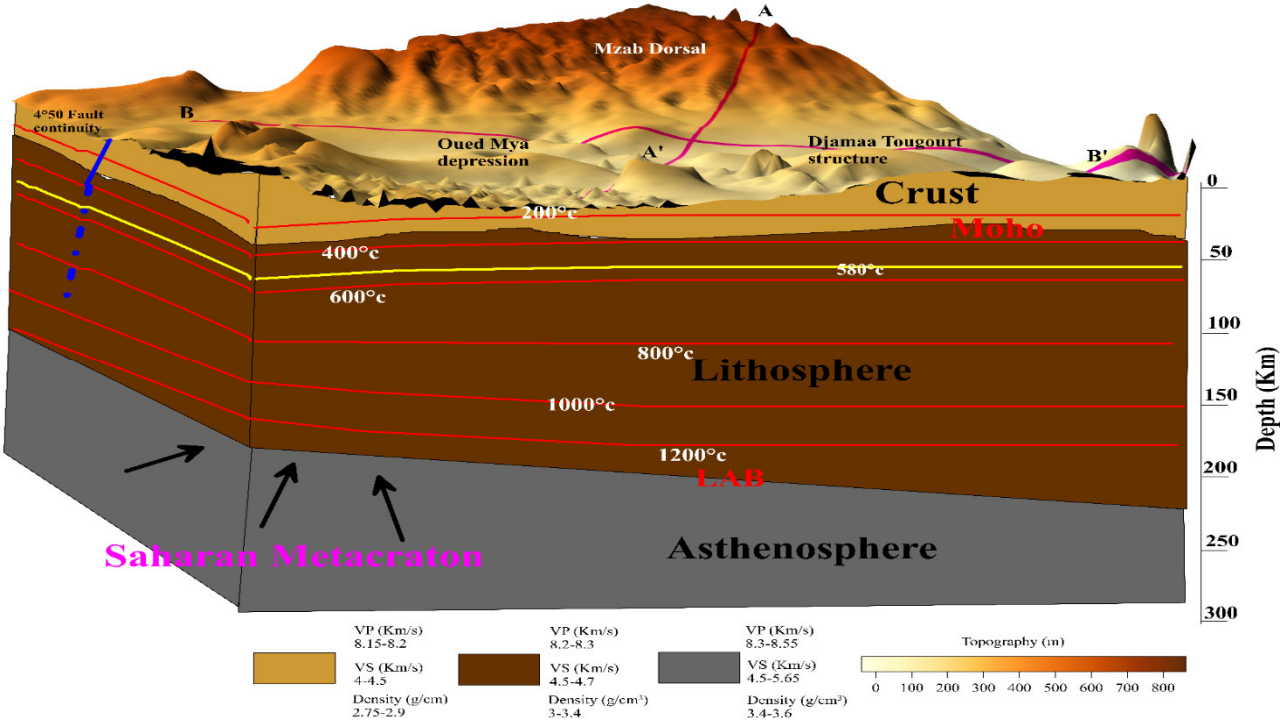


**[Fig.08]**:Thermo-structural model of the Triassic province based on multi-scale geophysical modeling approach: The Curie isotherm at 580°C is defined by yellow contour line , the red contours represent the distribution of temperature through the crust-mantle layers, the blue line represents the M'zab fault system, and the black arrows represent the deformation generated by the Saharan metacratonic movements.

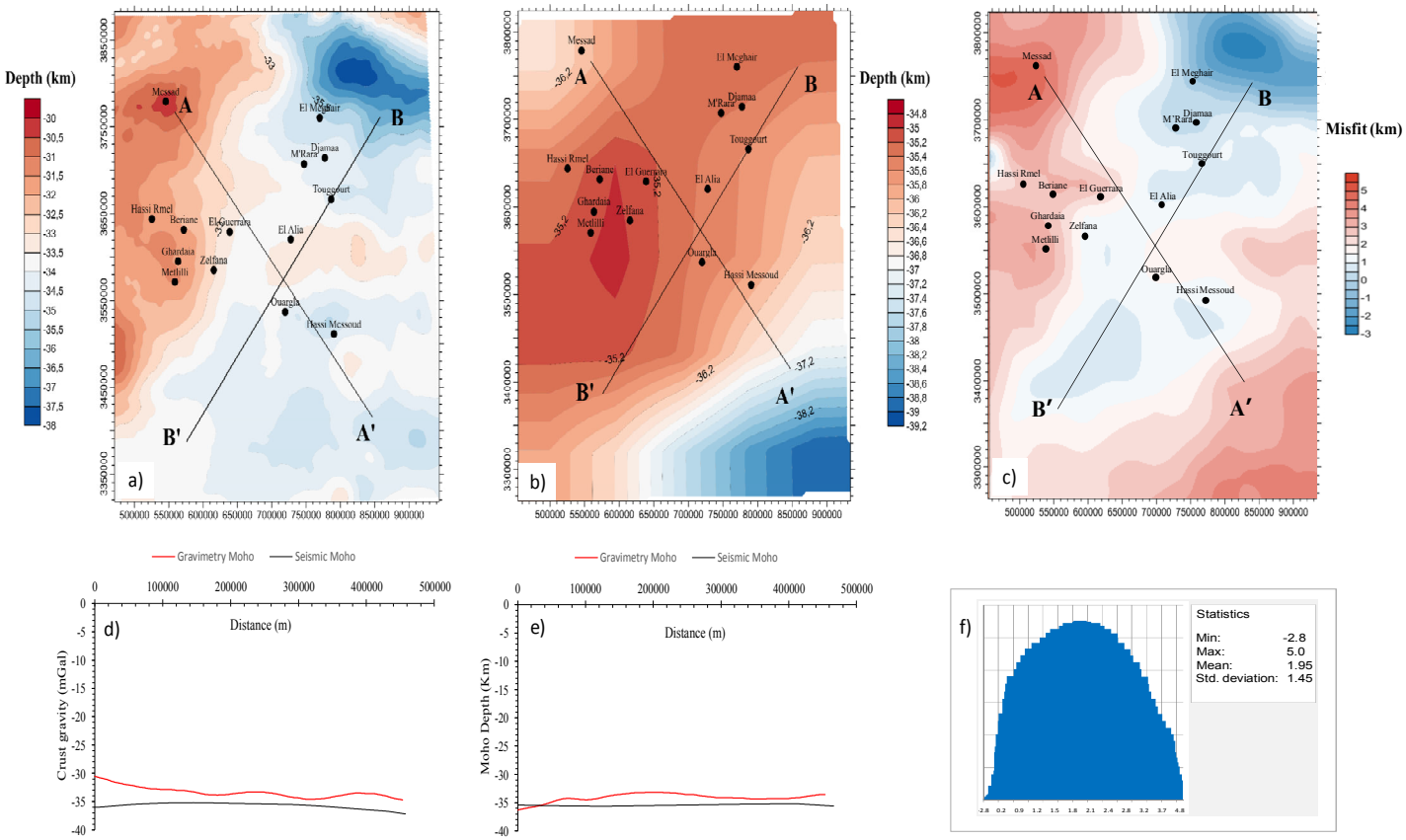


**[Fig. 09]:** (a) Gravimetric Moho depth model, (b) Seismic derived Moho depth model from CRUST 1.0, (c) calculated misfit between the gravimetric Moho model and the Crust 1.0 derived depth to Moho model, (d) A-A' cross-section of the gravimetric and seismic Moho depths, (e) B-B' cross-section of the gravimetric and seismic Moho depths, (f) misfit of the gravimetric and seismic derived CRUST 1.0 models

# conclusion

# CONCLUSION

## Conclusion

The analysis of structural observations combined with gravity and magnetic data has provided new insights into the crustal architecture of the Triassic province. This research employed two approaches, utilizing the LitMod-2D modeling code and empirical relationships, to decipher the architecture of the lithospheric and asthenospheric layers. The results highlight the influence of compressional movements of the Saharan metacraton, resulting in thinner lithosphere-asthenosphere boundary (LAB) beneath Berkine and Ghadames basins and thicker LAB beneath the M'zab dorsal and surrounding zones. Additionally, thermal inversion revealed the depth range of the Curie isotherm, indicative of deep geothermal reservoirs.

Updates on geologic knowledge through 2D seismic velocity and thermal models revealed distinctive variability in density, seismic velocities, and temperature distributions of lithosphere and asthenosphere structures, precluding the initial concept of geothermal field origin from lower mantle plume contamination. Instead, geothermal reservoirs are interpreted as results of localized disturbance within the crust-uppermost mantle interface, leading to hot plumes ascending through probable deep fault systems. This provides novel interpretations for the origin of Albian hydrothermal reservoirs and insights into lithosphere-asthenosphere structure within the Saharan platform.

Comparative analysis of gravimetric Moho and CRUST 1.0 model revealed minimal misfit, indicating the reliability of the gravimetric Moho model within the Saharan platform. Discrepancies were attributed to the inability of the seismic Moho model to capture major geologic realities due to low seismic data coverage. Hence, in regions with low seismic data coverage, gravimetric Moho provides more detailed information for updating CRUST 1.0 model. The validation results suggest that the data reduction procedure and applied approach are reliable and can be applied elsewhere in regions with similar geodynamic scenarios to improve understanding of subsurface thermo-structural properties and dynamics. Despite uncertainties in crustal and lithospheric mantle compositions within the Saharan platform due to paucity of petrological/geochemical data, the model presents novel insights into lithospheric-asthenospheric properties within the Saharan platform.

# Références

# REFERENCES

**References**


Afonso, J. C. (2006). Thermal, density, seismological, and rheological structure of the lithospheric-sublithospheric mantle from combined petrological-geophysical modelling: Insights on lithospheric stability and the initiation of subduction, Ph.D. thesis, Carleton Univ., Ottawa, Ontario, Canada. (Available at :

http://wija.ija.csic.es/gt/afonso/homepage.htm)

Afonso, J. C., Fernandez, M., Ranalli, G., Griffin, W. L., Connolly, J. A. D. (2008). Integrated geophysical-petrological modeling of the lithosphere and sublithospheric upper mantle: methodeologie and applications. Geochemistry, Geophysics, Geosystems. 9(5), Q05008, doi:10.1029/2007GC001834

Afonso, J. C., &Ranalli, G. (2004). Crustal and mantle strengths in continental lithosphere: is the jelly sandwich model obsolete?. *Tectonophysics*, *394*(3-4), 221-232.

Afonso, J. C., Salajegheh, F., Szwillus, W., Ebbing, J., Gaina, C. (2019). A global reference model of the lithosphere and upper mantle from joint inversion and analysis of multiple data sets. Geophys, J. Int, 217(3), 1602-1628.

Ai, Y., Zhang, J., Dong, M., Wang, B., & Fang, G. (2021). Heat generation effects from shear friction along Xianshui river strike-slip fault in western Sichuan, China. *Geothermics*, *89*, 101936.

Al-Douri, Y., Waheeb, S. A., & Johan, M. R. (2019). Exploiting of geothermal energy reserve and potential in Saudi Arabia: A case study at Ain Al Harrah. Energy reports, 5, 632-638. https://doi.org/10.1016/j.egyr.2019.05.005

Ali, S. M., Abdelrahman, K. (2022). Earthquake Occurrences of the Major Tectonic Terranes for the Arabian Shield and Their Seismic Hazard Implications. Frontiers in Earth science. 10, 851737.

Alrefaee, H. A., Soliman, M. R., Merghelani, T. A. (2022). Interpretation of the subsurface tectonic settings of the Natron basin, North Western desert, Egypt using Satellite Bouguer gravity and magnetic data. Journal of African Earth sciences, 187, 104450.https://doi.org/10.1016/j.jafrearsci.2022.104450

# REFERENCES


Artemieva, I.M., and Mooney, W.D., (2001). Thermal structure and evolution of Precambrian lithosphere: A global study. J. Geophys. Res, 106, 16387-16414

Artemieva, I. M., and Vinnik, L.P., (2016). Density structure of the cratonic mantle in southern Africa: 2. Correlations with seismic velocities, kimberlite distribution, and tectonics. Gondwana Research, 36, 14-27. https://doi.org/10.1016/j.gr.2016.05.002

Aydemir, A., Bilim, F., Kosaroglu, S., & Buyuksarac, A. (2019). Thermal structure of the Cappadocia region, Turkey: a review with geophysical methods. Med. Geosc. Rev. **1,** 243–254. https://doi.org/10.1007/s42990-019-00011-7

Bertrand, J. M. L. and Caby, R. (1978). Geodynamic evolution of the Pan-African orogenic belt: A new interpretation of the Hoggar shield (Algerian Sahara), Geol. Rundsch., 67(2), 357–388, doi:10.1007/BF01802795.

Bhattacharyya, B. K., &Leu, L. K. (1975). Analysis of magnetic anomalies over Yellowstone National Park: mapping of Curie point isothermal surface for geothermal reconnaissance. *Journal of Geophysical Research*, *80*(32), 4461-4465.Bian, M., Kamenskii, A. N., Han, M., et al. (2021). Covalent 2D $Cr_2Te_3$ferromagnet. Mater. Res. Lett. 9, 205-212.

Bilim, F., Aydemir, A., Kosaroglu, S., &Bektas, O. (2018). Effects of the Karacadag Volcanic Complex on the thermal structure and geothermal potential of southeast Anatolia. Bull Volcanol, 80.https://doi.org/10.1007/s00445-018-1228-y

Bilim, F., Aydemir, A., &Ates, A. (2021a). Interpretation of aeromagnetic data for the geothermal properties in the northwestern part of Turkey. Journal of African Earth Sci, 177, 104148. https://doi.org/10.1016/j.jafrearsci.2021.104148

Bilim, F., Aydemir, A., Ates, A., Nuri Dolmaz, M., Koşaroğlu, S., &Erbek, E. (2021b). Crustal thickness in the Black Sea and surrounding region, estimated from the gravity data. Marine and Petroleum Geology, 123, 104735. https://doi.org/10.1016/j.marpetgeo.2020.104735

# REFERENCES


Black, R., Liégeois, J.P. (1993) Cratons, Mobile Belts, Alkaline Rocks and Continental Lithospheric Mantle: The Pan-African Testimony. Journal of the Geological Society, 150, 89-98.http://dx.doi.org/10.1144/gsjgs.150.1.0088

Boone, S. C., Balestrieri, M. L., Kohn, B. (2021). Tectono-Thermal evolution of the Red sea Rift. Front. Earth sci. 9, 713448.

Buness, H., Giese, P., Bobier, C., Eva, C., Merlanti, F., Pedone, R., Jenatton, L., Nguyen, D.T., Thouvenot, F., Egloff, F. &Makris, J. (1992). The EGT-85 Seismic Experiment in Tunisia-a reconnaissance of the deep structures. *Tectonophysics*, *207*(1-2),245-267.

Caby, R., Andreopoulos-Renaud. (1987). Le hoggar orientale, block cratonisé a 730 Ma dans la chaine pan-africaine du nord du continent africain, Precambrianresearch. 36(3-4), 335-344.

Chai, C., Ammon, C .J., Maceira, M., Herrmann, R. (2022). Crust and upper mantle structure beneath the eastern United States. Geochemistry, Geophysics, Geosystems. 23(3), e2021GC010233. https://doi.org/10.1029/2021GC010233

Chakraborty, K., Agarwal, B. N. P. (1992). Mapping of crustal discontinuities by wavelength filtering of the gravity field 1. *Geophysical prospecting*, *40*(7), 801-822.

Chopping, R., Kennett, B. L. (2015). Maximum depth of magnetisation of Australia, its uncertainty, and implications for Curie depth. GeoResJ, 7, 70-77.

Dostal, J., Caby, R., Keppie, J., 2002. Neoproterozoic magmatism in Southwestern Algeria (SebkhaelMelah inlier): a northerly extension of the Trans-Saharan orogen. J. Afr. Earth Sci. 35 (2), 213–225. https://doi.org/10.1016/S0899-5362(02)00104-

Elbarbary, S., Abdel Zaher, M., Saibi, H., Fowler, A., Ravat, D., Marzouk, H. (2022). Thermal structure of the African continent based on magnetic data: Future geothermal renewable energy exploration in Africa. Renewable and Sustainable Energy Reviews. 158, 112088. https://doi.org/10.1016/j.rser.2022.112088

Eldosouky, A.M., Elkhateeb, S.O., Mahdy, A.M., Saad, A.A., Fnais, M.S., Abdelrahman, K., Andráš, P. (2022). Structural analysis and basement topography of GabalShilman area, South Eastern Desert of Egypt, using aeromagnetic data. Journal of King Saud University - Science, 34(2), 101764. https://doi.org/10.1016/j.jksus.2021.101764.

# REFERENCES


Fabre, J., (1976). Introduction à la géologie du Sahara algérien. S.N.E.D Algeriers, Algeria.

Fekirine, B.,Murty, D. A. (2003). Cambro-Ordovician Sequence Stratigraphy of the Saharan Platform, Algeria. *In,* Proceedings of the AAPG Algiers Research Conference on Palaeozoic and Triassic Petroleum Systems in North Africa, February 18-20, 2003, Algiers, Algeria.

Fernandez, M., Afonso, J.C., Ranalli, G. (2010). The deep lithospheric structure of the Namibian volcanic margin,Tectonophysics, 481(1-4), 68-81. https://doi.org/10.1016/j.tecto.2009.02.036

Fullea, J., Afonso, J. C., Connolly, J. A. D., Fernandez, M., García-Castellanos, D., &Zeyen, H. (2009). LitMod3D: An interactive 3-D software to model the thermal, compositional, density, seismological, and rheological structure of the lithosphere and sublithospheric upper mantle. *Geochemistry, Geophysics, Geosystems*, *10*(8).

Fullea, J., Fernandez, M., &Zeyen, H. (2008). FA2BOUG—A FORTRAN 90 code to compute Bouguer gravity anomalies from gridded free-air anomalies: Application to the Atlantic-Mediterranean transition zone. *Computers & Geosciences*, *34*(12), 1665-1681.

Fullea, J., M. Fernandez, H. Zeyen, and J. Verge´s. (2007). A rapid method to map the crustal and lithospheric thickness using elevation, geoid anomaly and thermal analysis. Application to the Gibraltar Arc System and adjacent zones, Tectonophysics, 430, 97-117, doi: 10.1016/j.tecto.2006.11.003.

Garcia, D., Ramillien, G., Lombard, A., &Cazenave, A. (2007). Steric sea-level variations inferred from combined Topex/Poseidon altimetry and GRACE gravimetry. In *Deformation and Gravity Change: Indicators of Isostasy, Tectonics, Volcanism, and Climate Change* (pp. 721-731). Birkhäuser Basel.

Globig, J., Fernàndez, M., Torne, M., Vergés, J., Robert, A., &Faccenna, C. (2016). New insights into the crust and lithospheric mantle structure of Africa from elevation, geoid, and thermal analysis. *Journal of Geophysical Research: Solid Earth*, *121*(7), 5389-5424.

Grenhölm, M., Jessell, M., Thébaud, N. (2019). A geodynamic model for the Paleoproterozoic (ca. 2.27-1.96 Ga) Birimianorogen of the southern West African

Craton-Insights into an evolving accretionary-collisional orogenic system. Earth Sci Rev, 192, 138-193

Griffin, W. L., & O'Reilly, S. Y. (2007). Cratonic lithospheric mantle: is anything subducted?. *Episodes Journal of International Geoscience*, *30*(1), 43-53.

Griffin, W. L., O'Reilly, S. Y., Afonso, J. C., &Begg, G. C. (2009). The composition and evolution of lithospheric mantle: a re-evaluation and its tectonic implications. *Journal of Petrology*, *50*(7), 1185-1204.

Hofmeister, A. M. (1999). Mantle values of thermal conductivity and the geotherm from phonon lifetimes, Science, 283,1699-1706.

Ikenne, M., et al., A historical overview of Moroccan magmatic events along northwest edge of the West African Craton, Journal of African Earth Sciences (2016), http://dx.doi.org/10.1016/j.jafrearsci.2016.10.002

Jaupart, C. (1983). Horizontal heat transfer due to radioactivity contrasts: causes and consequences of the linear heat flow relation. *Geophysical Journal International*, *75*(2), 411-435.

Jiang, Y., Jiang, S., Li, S., Wang, G., Zhang, W., Lu, L., Guo, L., Liu, Y.,& Santosh, M. (2022). Paleozoic to Mesozoic micro-block tectonics in the eastern central Asian Orogenic belt: Insights from magnetic and gravity anomalies. Gondwana research, 102,229-251.

Kaban, M.K., El Khrepy, S. & Al-Arifi, N. (2017). Importance of the Decompensative Correction of the Gravity Field for Study of the Upper Crust: Application to the Arabian Plate and Surroundings. Pure Appl. Geophys. 174**,** 349-358. https://doi.org/10.1007/s00024-016-1382-0

Kedaid, F.Z., (2007). Database on the geothermal resources of Algeria, Geothermics, 36(3), 265-275. https://doi.org/10.1016/j.geothermics.2007.02.002

Khudier, A. A., Paquette, J. L., Nicholson, K., Johansson, Å., Rooney, T. O., Hamid, S., El-Fadly, M.A, Corcoran, L, Malone S.J. & El-Rus, M. A. A. (2021). On the

cratonizationof the Arabian-Nubian Shield: Constraints from gneissic granitoids in south Eastern Desert, Egypt. GeoscienceFrontiers, 12(4), 101148.

Kourim, F., Bodinier, J.L., Alard, O., Bendaoud, A., Vauchez, A., Dautria, J.M. (2014). Nature and Evolution of the Lithospheric Mantle beneath the Hoggar Swell (Algeria): a Record from Mantle Xenoliths. Journal of petrology, 55(11), 2249-2280. https://doi.org/10.1093/petrology/egu056

Lachenbruch, A. H., and Morgan, P. (1990). Continental extension, magmatism and elevation; formal relations and rules of humb, Tectonophysics, 174, 39-62, doi:10.1016/0040-1951(90)90383-J.

Lamali, A., Merabet, N., Henry, B., Maouche, S., Graine-Tazerout, K., Mekkaoui, A., Ayache, M., (2013). Polyphased geodynamical evolution of the Ougarta (Algeria) magmatic complexes evidenced by paleomagnetic and AMS studies. Tectophysics 558, 82–99. https://doi.org/10.1016/j.tecto.2012.12.007.

Lambert-Smith, J.S., Lawrence, D.M., Müller, W., Treloar, P.J. (2016). Paleotectonic setting of the south-eastern Kédougou-Kénieba inlier, West Africa: new insights from igneous trace element geochemistry and U-Pb zircon ages. PrecambrRes 274, 110-135

La Rosa, A., Pagli, C., Wang, H., Doubre, C., Leroy, S., Sani, F., Corti, G., Ayele, A., &Keir, D. (2021). Plate-Boundary kinematics of the Afrera linkage zone (Afar) from InSAR and Seismicity. Journal of Geophysical Research: Solid Earth, 126, e2020JB021387. https://doi. org/10.1029/2020JB021387

Lefort, J. P., & Agarwal, B. N. P. (2000). Gravity and geomorphological evidence for a large crustal bulge cutting across Brittany (France): a tectonic response to the closure of the Bay of Biscay. *Tectonophysics*, *323*(3-4), 149-162.

Lesquer, A., Beltrao, J.F., De Abreu, F.A.M., 1984. Proterozoic links between northeastern Brazil and West Africa: a plate tectonic model based on gravity data. Tectonophysics 110(1-2), 9-26. https://doi.org/10.1016/0040-1951(84)90055-6

Liégeois, J.P., Benhallou, A., Azzouni-Sekkal, A., Yahiaoui, R., and Bonin, B. (2005). The Hoggar swell and volcanism: Reactivation of the Precambrian Tuareg shield during Alpine convergence and West African Cenozoic volcanism, in Foulger, G.R., Natland,

J.H., Presnall, D.C., and Anderson, D.L., eds., Plates, Plumes and Paradigms: Geological Society of America Special Paper 388, p. 379-400

Liégeois, J. P., Sauvage, J. F. and Black, R. (1991). The Permo-Jurassic alkaline province of Tadhak, Mali: Geology, geochronology and tectonic significance, Lithos, 27(2), 95–105, doi:10.1016/0024-4937(91)90022-D.

Liu, J., Pearson, D.G., Wang, L.H. *et al.* (2021). Plume-driven recratonization of deep continental lithospheric mantle. *Nature*, **592,** 732–736. https://doi.org/10.1038/s41586-021-03395-5

Maddaloni, F., Pivetta, T., Braitenberg, C. (2021). Gravimetry and petrophysics for defining the intracratonic and rift basins of the Western-Central Africa zone. Geophysics. 86(6), B369.

Masurel, Q., Thébaud, N., Miller, J., Ulrich, S., Roberts, M.P., Béziat, D. (2017). The Alamoutala carbonate-hosted gold deposit, Kédougou-Kénieba inlier, West Africa. Econ Geol, 112, 49-72

Meghraoui, M., Abdellaoui, H., Masson, F. (2021). Constraint of Active Deformation between the African Platform and the Maghrebian Thrust Belt: Current Plate Motion from Permanent GNSS data in Algeria. In *EGU General Assembly Conference Abstracts* (pp. EGU21-12969).

Mekkaoui, A., Remaci-Benaouda, N., Graine-Tazerout, K., (2017). Mafic dikes at KahelTabelbala (Daoura, Ougarta Range, south-western Algeria): new insights into the petrology, geochemistry and mantle source characteristics. C.R. Geoscience 349 (5), 202–211. https://doi.org/10.1016/j.crte.2017.06.003.

Melouah, O., & Pham, L. T. (2021). An improved ILTHG method for edge enhancement of geological structures: application to gravity data from the OuedRigh valley. Journal of African Earth Sciences. 177, 104162. https://doi.org/10.1016/j.jafrearsci.2021.104162

Melouah, O., Eldosouky, A. M., &Ebong, E. D. (2021a). Crustal architecture, heattransfer modes and geothermal energy potentials of the Algerian Triassic provinces. Geothermics. 96, 102211. https://doi.org/10.1016/j.geothermics.2021.102211.

# REFERENCES


Melouah, O., Lopez Steinmetz, R. L., &Ebong, E. D. (2021b). Deep crustal architecture of the eastern limit of the West African Craton: Ougarta Range and Western Algerian Sahara. Journal of African Earth Sciences. 183,104321.

https://doi.org/10.1016/j.jafrearsci.2021.104321

Mukhopadhyay, M., Mukhopadhyay, B., Mogren, S., et al. (2022). Regional significance of crustal and sub-crustal rheological heterogeneities beneath the HarratLunayyir and their continuity into the neighboring harrats, Western Saudi Arabia -Perspectives of the Afar plume activity. Journal of African Earth Sciences. 186, 104432, https://doi.org/10.1016/j.jafrearsci.2021.104432.

Ockendon, J. R., &Turcotte, D. L. (1977). On the gravitational potential and field anomalies due to thin mass layers. *Geophysical Journal International*, *48*(3), 479-492.

O'Reilly, S. Y., & Griffin, W. L. (2006). Imaging global chemical and thermal heterogeneity in the subcontinental lithospheric mantle with garnets and xenoliths: Geophysical implications. *Tectonophysics*, *416*(1-4), 289-309.

O'Reilly, S. Y., Griffin, W. L., Djomani, Y. H. P., & Morgan, P. (2001). Are lithospheres forever? Tracking changes in subcontinental lithospheric mantle through time. *GSA today*, *11*(4), 4-10.

Pasyanos, M.E., &Walter, W.R. (2002). Crust and upper-mantle structure of North Africa, Europe and the Middle East from inversion of surface waves. Geophys. J. Int, 149, 463-481.

Pavlis, N. K., Holmes, S. A., Kenyon, S. C., & Factor, J. K. (2012). The development and evaluation of the Earth Gravitational Model 2008 (EGM2008). *Journal of Geophysical Research: Solid Earth*, *117*(B4).

Perron, P. (2019). Architecture and tectonic of Paleozoicintracratonic Basins: Impact on the sedimentary record and associated geometries. Example of peri-Hoggar Basins (North Gondwana marge). Université de Bourgogne franchecomte, Pp397.

Petitjean, S., Rabinowicz, M., Grégoire, M., &Chevrot, S. (2006). Differences between Archean and Proterozoic lithospheres: Assessment of the possible major role of thermal conductivity. *Geochemistry, Geophysics, Geosystems*, *7*(3).

# REFERENCES


Poudjom-Djomani, Y.H., O,' Reilly, S.Y., Griffin, W.L., Morgan, P. (2001). The density structure of subcontinental lithosphere through time. Earth Planet. Sci. Lett. 184, 605-621.

Riad, S., Refai, E., &Ghalib, M. (1981). Bouguer anomalies and crustal structure in the Eastern Mediterranean. *Tectonophysics*, *71*(1-4), 253-266.

Rudnick, R.L., Barth, M.G., McDonough, W.F., Horn, I. (1998). Rutiles in eclogites: a missing Earth reservoir found? GSA Abstr. 30 (7), A-207, Toronto

Saibi, H., 2009. Geothermal resources in Algeria, Renewable and Sustainable Energy Reviews, 13(9), 2544-2552.

Sandvol, E., Seber, D., Calvert, A., &Barazangi, M. (1998). Grid search modeling of receiver functions: Implications for crustal structure in the Middle East and North Africa. *Journal of Geophysical Research: Solid Earth*, *103*(B11), 26899-26917.

Sandwell, D. T., Garcia, E. M., Smith, W. H., Soofi, K., Wessel, P., & Francis, R. (2013). Towards 1 MilliGal Global Marine Gravity Accuracy from CryoSat-2, Jason-1, and Envisat. In *AGU Fall Meeting Abstracts* (Vol. 2013, pp. G53C-08).

Shehata, M. A., &Mizunaga, H. (2022). Moho depth and tectonic implications of the western United States: insights from gravity data interpretation. *Geoscience Letters*, *9*(1), 1-15.

Shulgin, A., &Artemieva, I. M. (2019). Thermochemical heterogeneity and density of continental and oceanic upper mantle in the European□North Atlantic region. Journal of Geophysical Research: Solid Earth, 124, 9280 – 9312. https://doi.org/10.1029/2018JB017025

Smith, W. H., &Sandwell, D. T. (1997). Global sea floor topography from satellite altimetry and ship depth soundings. *Science*, *277*(5334), 1956-1962.

Sobh, M., Ebbing, J., Mansi, A. H., Gotze, H.-J., Emry, E., &Abdelsalam, M. (2020). The lithospheric structure of the Saharan metacraton from 3-D integrated geophysical-petrological modeling. Journal of Geophysical Research: Solid Earth, 125(8), e2019JB018747. https://doi.org/10.1029/2019jb018747

Sprague, A. R. (1991). Depositional sequence evolution, Paleozoic and early Mesozoic of the central Saharan platform, North Africa. *Geobyte;(United States)*, *75*(CONF-910978-).

# REFERENCES


Stephenson, R., Egholm, D. L., Nielsen, S. B., &Stovba, S. M. (2009). Role of thermal refraction in localizing intraplate deformation in southeastern Ukraine. *Nature Geoscience*, *2*(4), 290-293.

Takherist, D., 1991. Structure crustale, subsidence mésozoïque et flux de chaleur dans les bassins nord-sahariens (Algérie): apport de la gravimétrie et des données de puits. Doctorat thesis, Montpellier university, France.

Tanaka, A., Okubo, Y., &Matsubayashi, O. (1999). Curie point depth based on spectrum analysis of the magnetic anomaly data in East and Southeast Asia. Tectonophysics, 306, 461-470. https://doi.org/10.1016/S0040-1951(99)00072-4.

Tašárová, A., Afonso, J. C., Bielik, M., et al. (2009). The lithospheric structure of the western Carpathian-Pannonian basin region based on the CELEBRATION 2000 seismic experiment and gravity modeling. Tectophysics, 475(3-4), 454-469.

Tunini, L., I. Jiménez-Munt, M. Fernandez, J. Vergés, A. Villaseñor, M. Melchiorre, and J. C. Afonso (2016), Geophysicalpetrological model of the crust and upper mantle in the India-Eurasia collision zone, Tectonics, 35, doi:10.1002/2016TC004161.

Van der Meijde, M., Fadel, I. E. A. M., Ditmar, P., &Hamayun, M. (2015). Uncertainties in crustal thickness models for data sparse environments: A review for South America and Africa. *Journal of Geodynamics*, *84*, 1-18.

Woollard, G.P., 1959. Crustal structure from gravity and seismic data measurements. Journal of Geophysical Research, 64(10), 1521-1544. https://doi.org/10.1029/JZ064i010p01521.

Xia, B., Thybo, H., &Artemieva, I. M. (2017). Seismic crustal structure of the North China Craton and surrounding area: Synthesis and analysis. Journal of Geophysical Research: Solid Earth, 122(7), 5181–5207. doi: 10.1002/2016JB013848

Xia, B., Thybo, H., &A rtemieva, I. M. (2020). Lithosphere Mantle Density of the North China Craton. Journal of Geophysical Research: Solid Earth, 125(9). doi:10.1029/2020jb020296

Yin, Y., Li, C-F.,& Lu, Y. (2021). Estimating Curie-point depths using both Wavlet-based and Fourier spectral centroid methods in the Western Pacific marginal seas. *Geophys. j.int. 227. 798*-812.

# REFERENCES

Zhang, Y.-Y., Chen, L., Wang, X., & Ai, Y.S., 2019, Lithospheric structure beneath the central and western North China Craton and adjacent regions from S-receiver function imaging, Geophysical Journal International, 219, 619-632. doi: 10.1093/gji/ggz322.

Zhang H, Zheng JP, Zhou YQ, Pan SK, Xiong Q, Lin AB, Zhao Y (2020) Mesozoic lithospheric modification and replacement beneath the Cathaysia block: mineral chemistry and water contents of the Daoxian peridotite xenoliths. Lithos 258–259:105385

Zheng, J., O'Reilly, S. Y., Griffin, W. L., Lu, F., Zhang, M., & Pearson, N. J. (2001). Relict refractory mantle beneath the eastern North China block: significance for lithosphere evolution. *Lithos*, *57*(1), 43-66.